HHS Public Access

Author manuscript

J Control Release. Author manuscript; available in PMC 2019 October 28.

Published in final edited form as:

J Control Release. 2018 October 28; 288: 111–125. doi:10.1016/j.jconrel.2018.09.003.

An Intestinal Paracellular Pathway Biased Toward Positively-Charged Macromolecules

Khaled Almansour[a], **Alistair Taverner**[a], **Jerrold R. Turner**[b], **Ian M. Eggleston**[a], and **Randall J. Mrsny**[a]

[a]Department of Pharmacy and Pharmacology, University of Bath, Bath BA2 7AY, UK

[b]Department of Pathology, Brigham and Women's Hospital and Harvard Medical School, Boston, MA 02115

Abstract

Lacking an effective mechanism to safely and consistently enhance macromolecular uptake across the intestinal epithelium, prospects for successful development of oral therapeutic peptide drugs remain unlikely. We previously addressed this challenge by identifying an endogenous mechanism that controls intestinal paracellular permeability that can be activated by a peptide, termed PIP 640, which can increase cellular levels of phosphorylated myosin light chain at position S^{19} (MLC-pS^{19}). Apical application *in vitro* or luminal application *in vivo* was shown to increase macromolecular solute transport within minutes that recovered completely within a few hours after removal. We now examine the nature of PIP 640-mediated permeability changes. Confluent Caco-2 cell monolayers treated with PIP 640 enhanced apicalto-basolateral (AB) transport of 4-kDa, but not 10-kDa, dextran. Expression and/or cellular distribution changes of tight junction (TJ) proteins were restricted to increased claudin-2 over a time course that correlated with an apparent shift in its distribution from the nucleus to the membrane fraction of the cell. PIP 640-mediated epithelial changes were distinct from the combined actions of the pro-inflammatory cytokines tumor necrosis factor alpha (TNF-α) and interferon gamma (IFN-γ). While TNF-α/IFN-γ treatment also increased MLC-pS^{19} levels, these cytokines enhanced AB transport for 70-kDa dextran and decreased occludin expression at TJs. Claudin-2-dependent changes induced by PIP 640 resulted in an AB transport bias for positively-charged macromolecules demonstrated *in vitro* using charge variants of 4-kDa dextrans and by comparing transport of salmon calcitonin to exenatide. Comparable outcomes of increased TJ localization of claudin-2 and enhanced transport of these therapeutic peptides that biased toward cationic characteristics was demonstrated *in vivo* following after intraluminal injection into rat jejunum. Together, these data have shown a potential mechanism for PIP 640 to enhance paracellular permeability of solutes in the size range of small therapeutic peptides that is biased toward positively-charged solutes.

Graphical Abstract

Contact Info: Prof. Randall Mrsny, University of Bath, Department of Pharmacy and Pharmacology, Claverton Down, Bath UK BA2 7AY, Tel +44 122 538 3358; Rjm37@bath.ac.uk.

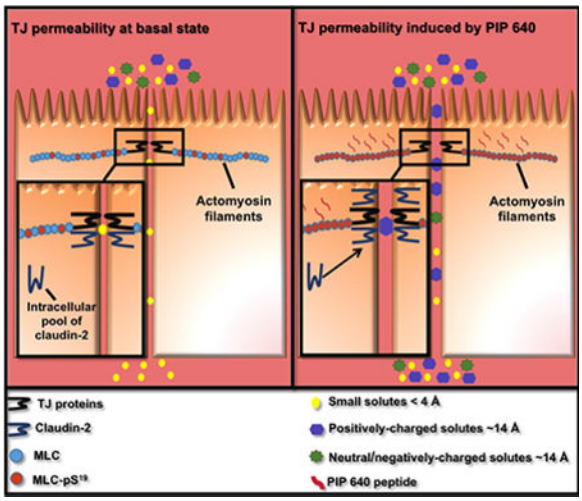

Keywords

Paracellular transport; myosin light chain phosphatase; insulin delivery; cell penetrating peptide; protein-protein interactions; tight junction function

Introduction

Intestinal epithelial cells are organized into distinct apical and basolateral compartments that are maintained by the apical junctional complex (AJC) [1]. The AJC consists of tight junction (TJ), adherens junction, and desmosomes, which work together to establish a close approximation of adjacent cell membranes at the apical neck of neighboring epithelial cells [2]. The TJ is a protein complex that segregates apical from basolateral plasma membrane lipid domains in each epithelial cell and restricts the movement of water, solutes, and ions through the space between adjacent epithelial cells; the so-called paracellular route [3]. A plethora of strategies have been tested with the goal of decreasing intestinal TJ barrier function to facilitate the paracellular uptake of orally administered therapeutic peptides [4]. Most of these approaches have been identified through empirical testing using *in vitro* cell models, followed by *in vivo* studies in rodents; formulations are commonly composed of dietary components or materials that are generally regarded as safe or deemed sufficiently safe for chronic administration [5]. While some of these approaches have reached clinical testing, their promising actions observed in rodents have failed to translate into effective actions in man, with <1% bioavailability and great variability typically being observed [6].

Many of these previous approaches to enhance paracellular permeability have lacked a clear mechanism of actions (MoA), even those that have been translated to clinical testing [7]. This lack of MoA limits the ability to effectively translate these approaches from pre-clinical to clinical testing to achieve safe and efficacious outcomes. A number of studies have recently provided MoA information for several of these enhancing approaches. For example, sodium caprate has been shown to destabilize and solubilize cell membranes, resulting in ATP depletion and cytoskeletal contraction through increased phosphorylation of myosin light chain (MLC), enhancing both transcellular and paracellular transport pathways across

intestinal epithelia [8]. It was also found that sodium caprate decreases tricellulin at tricellular TJ structures and claudin-5 at bicellular structures, with the greater impact on enhancing paracellular permeability occurring at tricellular locations [9]. Other strategies have examined how certain pathogens can down-regulate bicellular TJ proteins such as occludin and claudins to disrupt the function of the paracellular barrier, with some attempting to recreate the actions of specific toxins secreted by certain pathogens to disrupt intestinal barrier function [10]. A recent example of this approach involves using an angulin binding fragment from the *Clostridium perfringens* iota-toxin, which causes the loss of angulin and tricellulin proteins from tricellular TJ structures [11]. By defining a specific MoA, one can directly probe safety and efficacy issues of promising approaches designed to enhance paracellular permeability that might limit their clinical utility due to possible pathophysiological outcomes through their chronic use.

As noted above, bacterial toxins and membrane disorganizing agents can result in the removal of critical proteins from TJ structures similar to inflammatory pathway activation, where recovery to homeostasis requires nascent protein biosynthesis and TJ integration [12, 13]. We have searched for a mechanism that might function on a faster dynamic scale and uses an endogenous pathway to modulated the paracellular properties of the intestinal mucosae. Specifically, we have explored the potential pharmaceutical application of a pathway activated by supra-physiological concentrations of nutrients in the intestinal lumen to transiently increase TJ permeability of peptides and polysaccharides [14]. This rapid and transient alteration of TJ permeability has been proposed as a physiological strategy that provides a secondary uptake route for nutrient uptake that complements continuous processes performed by transporters for essential amino acids and glucose present in at the apical membrane of enterocytes [15, 16]. Similar to that observed for studies with sodium caprate, the mechanism by which Na^+-nutrient cotransport enhances TJ permeability involves increased MLC phosphorylation [17, 18]. We have described a peptide, termed PIP 640, that can transiently increase myosin light chain phosphorylation at serine 19 (MLC-pS^{19}) to stimulate a TJassociated actomyosin filament contraction to recreate the actions of supra-physiological concentrations of nutrients that acts to dynamically diminish barrier function [19]. Most recently, we have performed positional assessment of amino acid requirements within the PIP 640 sequence to better define its capability to enter intestinal epithelial cells, localize to TJ structures, and interact with MLC phosphatase elements in order to further validate its anticipated MoA [20].

The current studies have examined TJ structure/function changes associated with PIP 640 treatment and evaluated size limitations of macromolecular solute uptake associated with these changes *via* the paracellular route assessed *in vitro* and *in vivo*. These studies show no significant decreases in TJ protein elements, like those observed for sodium caprate or the *Clostridium perfringens* iota-toxin. Oppositely, PIP 640 increased cellular levels of only one TJ protein: claudin-2. Increased levels of claudin-2 have been correlated with paracellular permeability changes that result in a bias toward cations [21]. Treatment with PIP 640 resulted in a similar charge bias, but which discriminated macromolecules in the size range of therapeutic peptides. Importantly, the time course of claudin-2 changes correlated with increased MLC-pS^{19} levels *in vitro* and *in vivo*. Changes induced by PIP 640 treatment rapidly recovered, consistent with the idea that this approach mimics the highly dynamic

changes associated with supra-physiological concentrations of nutrients in the intestinal lumen [14]. In sum, these data provide a deeper understanding of the PIP 640 MoA and how this agent might be used to transiently enhance the uptake of therapeutic peptides through a process that involves an endogenous pathway where specific physicochemical properties of the transporting solute can affect its movement through the paracellular route.

Materials and Methods

Peptide synthesis

PIP peptides were synthesized as described previously using an automated Symphony Quartet peptide synthesizer (Gyros Protein Technologies, USA) with Fmoc-protected D-amino acids on Rink amide MBHA resin (0.6 mmol/g loading) (Novabiochem, UK) [20]. First amino acid loading onto the resin was performed manually with N,N'-diisopropylcarbodiimide and 1hydroxybenzotriazole as coupling agents in the presence of diisopropylethylamine (DIEA) (Sigma-Aldrich, UK), with assembly of the remaining amino acids being performed automatically by the peptide synthesizer using (benzotriazol-1-yloxy)-tripyrrolidinophosphonium hexafluorophosphate (Novabiochem, UK) as the coupling reagent with DIEA. Crude peptides were cleaved and characterized using the same reagents and conditions described previously (Taverner, 2015).

Cell Culture and pro-inflammatory cytokines treatments

Caco-2BBe cell line was used to perform all *in vitro* cell-based studies. Cells were maintained as described previously using DMEM medium supplemented with 10% of FBS (Fisher Scientific, UK) and 1% of an antibiotic mixture containing penicillin (100 unit/mL) and streptomycin (100 μg/mL) (Sigma-Aldrich, UK), being cultured on 1.2 cm^2 (0.4 μm pore size) polyester membranes of 12-well Transwell® plates (Sigma-Aldrich, UK) at a cell density of 7×10^4/well at 37°C to reach polarization to achieve a trans-epithelial electrical resistance (TEER) value of > ~350 Ω·cm^2 that typically occurred in ~2 weeks [20]. A stable claudin-2 knock-down Caco-2 cell line (Caco-2-Cldn2$^{-/-}$) and control cells were maintained and used in polarized formats as described [21]. Induction of TJ barrier loss by basolateral treatment of Caco-2 monolayers with 10 ng/mL IFN-γ overnight prior to addition of 5 ng/mL TNF-α for 4 h (Fisher Scientific, UK) was performed as described [22]. PIP peptides were applied on the apical compartments of cell monolayers as described in [20].

Immunoblotting analysis

Total lysates of cell monolayers and rat intestinal tissues were prepared as described previously [19, 20]. Nuclear and membrane fractions of cell monolayers were collected using a commercial kit (Thermo Scientific, UK). Collected total/subcellular materials were diluted with electrophoresis sample buffer in a 1:1 ratio and separated by SDS-PAGE prior to transfer onto PDVF membrane and antibody probing [20]. Proteins of interest were probed using primary antibodies against claudin-1, claudin-2, claudin-3, claudin-4, claudin 7, claudin-8, occludin, total MLC (Abcam, UK), actin, cludin-15, claudin-5, MARVELD3 (Santa Cruz Biotech, UK), tricellulin, ZO-1 (Invitrogen, UK), and phospho-MLC (Ser19) (Cell Signaling Technologies, UK). Proteins were detected using LI-COR antibodies, as

described previously [20]. Images were collected using the Odyssey CLX imager (LI-COR, UK) and analyzed using the Image Studio Lite software, version 5.2.

Immunofluorescence staining

Cell monolayers were washed thrice with 500 μL of HBSS after PIP peptides treatments, then washed once with the same volume of ice-cold MeOH prior to being fixed by placing in precooled MeOH at −20°C for 1 h. Cell monolayers were then re-hydrated by incubation in phosphate buffer saline (PBS) for 15 min at room temperature (RT) before being blocked with 10% (v/v) FBS in PBS for 1 h at RT. Monolayers were then washed thrice with PBS that followed by a 1 h incubation at RT with secondary antibodies-conjugated to Alexa Fluor® 546 or Alexa Fluor® 488 (Invitrogen, UK). Cell monolayer were then washed thrice with PBS and mounted on microscope slides, as described previously [20]. Rat intestinal tissues, exposed to PIP 640 via intraluminal injections (ILI) into rat mid-jejunum, were isolated as described previously [19]. Tissues were fixed with 4 % paraformaldehyde, embedded in paraffin, and allowed to set at 4°C overnight. Paraffin-embedded tissues were sectioned to obtain 5 μm slices that were placed onto glass slides. Tissues were then immune-stained with fluorescent antibodies, described above. Images were collected using a Zeiss LSM 510 confocal microscopy.

Analysis of epithelial barrier function *in vitro*

Epithelial barrier property changes *in vitro* were evaluated by monitoring trans-epithelial electrical resistance (TEER) and measuring transport of 4 kDa fluorescein isothiocyanate (FITC)-dextran, 10 kDa FITC-dextran, 70 kDa tetramethylrhodamine isothiocyanate (TRITC)dextran (Sigma-Aldrich, UK), salmon calcitonin (Novabiochem, UK) and exenatide (Tocris Bioscience, UK) over 1 h from the apical to basal compartment of Transwell® plates with polarized Caco-2 cell monolayers [20]. Apical to basolateral permeability of dextran having different net charge was performed using positively-charged FITC-diethylaminoethyl-dextran (FITC-DEAE-dextran) or negatively-charged FITC-carboxymethyl-dextran (FITC-CM-dextran) with comparison to neutral TRITC-dextran (Sigma-Aldrich, UK), all having an average molecular weight of 4 kDa and prepared at a stock working concentration of 1 mg/mL. The apical concentration of salmon calcitonin and exenatide used was 5 μg/mL and contained 20 μg/mL of soybean trypsin inhibitor (SBTI). Samples of salmon calcitonin and exenatide collected from the basal compartment were analysed using an EIA Kit (Phoenix Pharmaceuticals, US) or an ELISA kit (2B Scientific Ltd, UK), respectively.

Assessment of enhanced permeability *in vivo*

All experiments were performed in accordance with the U.K. Animals (Scientific Procedures) Act of 1986, the European Communities Council Directive of 1986 (86/609/EEC), and the University of Bath's ethical review procedures. Rats were anesthetized and their abdominal cavity accessed via a midline surgical incision to allow ILI and blood sample collection from the portal vein [19]. ILIs (50 μL) were performed for solutions containing either salmon calcitonin (Novabiochem, UK) or exenatide (Tocris Bioscience, UK) (0.5 mg) with or without 20 mM PIP 640; in all cases, 1.5 mg/mL SBTI (Sigma-Aldrich, UK) was included help stabilize the therapeutic peptide. Blood samples (100 μL)

were collected at set time points from the portal vein and placed into Eppendorf tubes containing 50 mM of EDTA (Fisher Scientific, UK) and 0.6 IU/mL aprotinin (Sigma-Aldrich, UK) to prevent blood coagulation and protein degradation, respectively. In all cases, 1.5 mg/mL soybean trypsin inhibitor (SBTI) (SigmaAldrich, UK) was included to help stabilize the therapeutic peptide. Blood samples were then centrifuged at 1,600 × *g* for 15 min at 4°C and the isolated plasma was stored at −80°C until use. Salmon calcitonin content in plasma samples was measured using an EIA Kit (Phoenix Pharmaceuticals, US), while exenatide was measured by ELISA (2B Scientific Ltd, UK). The same plasma samples were also examined for endotoxin levels using a semi-quantitative E-Toxate™ *Limulus amebocyte* lysate (LAL) assay kit (Sigma-Aldrich, UK). Hydrodynamic radii of peptides were calculated using the following relationship

$$RH = \left[\frac{3\,MW}{4\,\pi\rho N}\right]^{\frac{1}{3}}$$

where RH in (cm), MW in (g/mol), ρ is the average density of a hydrated protein (0.99 g/cm3), N is Avogadro's number (6.02×10^{23}/mol), which assumes a spherical peptide shape in solution [23].

Data Analysis

All data are represented as means ± SEM of independent experiments. A two-tailed unpaired t-test was used for comparison between two groups. Potential differences between treatment groups were examined using one-way ANOVA; Tukey's multiple comparison was used to test for experiments involving three or more treatments. All statistical analysis was performed using GraphPad Prism® software version 7. Pharmacokinetic (PK) analysis was performed using Microsoft Excel add-in program, PK solver version 2.0 [24].

Results

PIP 640 selectively increases total level of claudin-2 and its distribution at TJ structures

Redistribution of TAMP protein family members (e.g. occludin, tricellulin, marvelD3) and the scaffolding protein ZO-1 are frequently associated with TJ modifications that result in increased large solute permeability across the intestinal epithelium [9, 25–27]. Therefore, we first examined the effect of a 60-min apical application of 1 mM PIP 640 on TAMPs and the associated scaffold protein ZO-1 using Caco-2 cell monolayers *in vitro* (Figs. 1A and B). Immunoblot analysis showed no significant changes in whole cell lysates levels of occludin, tricellulin, marvelD3, and ZO-1 in association with increase in MLC-pS^{19} induced by PIP 640. Further, apical PIP 640 treatment of confluent Caco-2 monolayers failed to demonstrate any striking changes to the cellular distribution of these TAMPs and ZO-1 proteins as assessed by immunofluorescent microscopy (Fig. 1C).

Although some claudins are recognised as paracellular ion channels [28], increases in macromolecular permeability across TJ barriers have also been associated with changes in expression or distribution of distinct claudin family members in health and disease [29, 30]. Therefore, we tested the hypothesis that the permeability enhancement induced by PIP 640

could be associated with changes in a specific set of claudins known to be expressed by intestinal epithelial cells [31, 32]. Polarized Caco-2 monolayers were exposed *in vitro* to a 60min apical treatment of 1 mM PIP 640. Of the claudins examined (claudin-1, −2, −3, −4, −5, −7, −8 and −15), only the claudin-2 displayed altered expression that coincided with increased MLCpS^{19} in response to PIP 640 (Figs. 2A and B). Importantly, claudin-2 levels were found to increase, suggesting an active process by these cells rather than a mechanism to destabilze or down-regulate a TJ element to faciliate enhanced paracellular permeability.

Immunoflourescence microscopy studies was performed to provide a more refined perspective of changes occurring to TJ-associated claudin proteins in response to PIP 640 (Fig. 3). A mixture of plasma membrane-associated and varying degrees of cytoplasmic distribution for claudin-1, −2, −4, and −7 was observed in untreated, polarized Caco-2 monolayers *in vitro*. After a 60-min apical application of 1 mM PIP 640, a greater intensity of cytoplasmic as well as plasma membrane immunostaining for claudin-2 was observed. No striking differences were observed in the intracellular or TJ distributions of claudin-1, −4 and −7 between the treated and untreated Caco-2 cell monolayers with the same concentration of the PIP 640 after 60 min. The observed increase in total claudin-2 cell levels demonstrated by Western blot analysis (Fig. 2) correlated with the increased levels of claudin-2 at the plasma membrane, presumably integrated into functional TJ structures (Fig. 3).

It has been shown that claudin-2 removed from TJ structures can be rapidly targeted to lysosomal degradation [33, 34]. Thus, it is possible that the relatively rapid (< 60 min) increase in total claudin-2 protein levels induced PIP 640 treatment may have been due, at least in part, to recruitment from cellular sites and/or stabilization via retention at TJ structures. We tested this hypothesis by examining the distribution of claudin-2 in polarized Caco-2 cell monolayers *in vitro* following a 60-min apical exposure to 1 mM PIP 640; the distribution of claudin-2 protein shifted from the nuclear fraction to the membrane fraction while occludin, a TJ protein that can co-localize with claudin-2 [35], did not undergo this same shift in response to PIP 640 during this time frame (Figs. 4). Together, these data are consistent with the hypothesis that PIP 640 actions facilitate the selective increase cellular claudin-2 levels, potentially through enhanced stability at TJs due to a shift in cellular pools toward the plasma membrane.

PIP 640 stimulates correlated increases in claudin-2 and MLC-pS^{19} levels

To better examine the potential relationship between increased claudin-2 levels at the plasma membrane and MLC-pS^{19} levels in response to 1 mM PIP 640, a time course study was performed that monitored these two parameters in correlation with Caco-2 cell monolayer trans-epithelial electrical resistance (TEER) values. Statistically-significant TEER reduction was detectable by 10 min after apical addition of PIP 640 with the effect becoming more pronounced over time and recovering fully following a washout after 60 min of exposure (Fig. 5A). This recovery would not be expected if, rather than regulating intercellular junctions, PIP 640 caused cell damage. Thus, the effects were not due to some type of intoxication mechanism. Further, this time course of response to and recovery from PIP 640 actions on Caco-2 monolayers *in vitro* was consistent with previous studies [19, 20]. Total

cellular levels of claudin-2 and MLC-pS^{19} levels examined over this time course of PIP 640 actions and recovery demonstrated that both claudin-2 and MLC-pS^{19} levels increase in a manner that coincided with rapid actions observed on TEER reduction (Figs. 5B and C). Of note, the time course for a detectable increase in total cell claudin-2 levels lagged slightly behind the more rapid increase in MLC-pS^{19} levels, consistent with a phosphorylation event or events that precede an increase in total cellular claudin-2 (Fig. 5C).

A time-course assessment of cellular claudin-2 distribution in Caco-2 monolayers *in vitro* after exposure to PIP 640 using immunofluorescence microscopy was performed to determine if the increase in claudin-2 levels detected by immunoblotting correlated with increased claudin-2 at the plasma membrane. Plasma membrane localization of claudin-2 increased over this time course in a manner consistent the findings showing a reduction in monolayer TEER and increases in total cellular levels of MLC-pS^{19} and claudin-2 levels (Fig. 6). This rapid onset of changes in the intracellular organization of claudin-2 and an increase in plasma membrane localization suggests claudin-2 redistribution from an intracellular pool to TJ structures in response to PIP 640 treatment rather than new protein. Removal of PIP 640 from Caco-2 monolayers after 60 min of apical treatment followed by overnight incubation with fresh medium led to complete recovery of claudin-2 distribution (Fig. 6).

To verify that the increase in claudin-2 at the plasma membrane (presumably at TJ structures) is a function of modulating MLC phosphatase (MLCP) activity by PIP 640, the actions of a PIP peptide mutant was examined. PIP 644 (sequence: rrrykvevrr-NH_2), where a single amino acid change in the PIP 640 sequence (highlighted in red), induces MLC-pS^{19} via an association with protein phosphatase 1 (PP1) instead of the MLCP complex, which composed of myosin phosphatase targeting subunit 1(MYPT1) and PP1, to produce a pronounced reduction of TJ barrier function that is not specific to MLCP [20]. Both PIP 640 and PIP 644 have been shown to increase MLC-pS^{19} levels and enhance paracellular permeability properties of Caco-2 monolayers *in vitro* [20]. Caco-2 monolayers treated with 1 mM PIP 640 or PIP 644 and examined after 10- and 60-min showed that while treatment with either peptide increased MLC-pS^{19} levels, only PIP 640 increased claudin-2 levels (Figs. 7A and B). Examination of total cellular occludin content in Caco-2 cell monolayers treated with 1 mM PIP 640 or PIP 644 and examined after 60 min showed that both peptides increased MLC-pS^{19} levels, but neither affected occludin levels (Figs. 7C and D). Immunofluorescence microscopy demonstrated that a 60-min apical application of 1 mM PIP 640 increased the distribution of claudin-2 at the plasma membrane of Caco-2 cells without a striking effect on occludin, while PIP 644 had no effect on claudin-2 or occludin plasma membrane levels (Fig. 7E).

PIP 640 actions are distinct from those of pro-inflammatory cytokines

Enhanced intestinal TJ permeability is commonly associated different intestinal inflammatory disorders, such as inflammatory bowel diseases (IBD), and such changes have been demonstrated to involve MLC-pS^{19} induction by prolonged activation of MLCK via actions of pro-inflammatory cytokines such as tumor necrosis factor-α (TNF-α) and interferon-γ (IFNγ) [12]. This process, in turn, results in rearrangement of TJ proteins, such

as induction of occludin endocytosis and/or claudin-2 upregulation, which results in increased TJ paracellular solute permeability properties that have been defined as the leak pathway [13]. The data presented above indicate that cellular changes induced by PIP 640 were associated with increased levels of claudin-2, presumably at TJ structures, that correlated with increased levels of MLC-pS^{19} levels similar to mechanisms demonstrated for TJ barrier dysfunction associated with IBD [36]. Thus, we compared the enhanced permeability properties resulting from PIP 640 to effects induced by pro-inflammatory cytokines (TNF-α/IFNγ) under conditions that have been demonstrated to drive the leak pathway associated with increased levels of MLC-pS^{19} levels and IBD-like conditions [37]. A decrease in TEER to ~70 % of the initial values occurred 60 min after an apical application of 1 mM PIP 640 to polarized Caco-2 monolayers *in vitro* (Fig. 8A), consistent with other studies described in this report (Fig. 5). This was compared to the actions of basal treatment with TNF-α/IFNγ for 4h to model the induction of an inflammation process [37], which resulted in a decrease in TEER to ~55 % of the initial values (Fig. 8A). While PIP 640 is designed to function following an apical application, the mechanism by which the proinflammatory cytokines TNF-α and IFNγ act to modulate MLC phosphorylation is through engagement of receptors expressed at the basal surface of intestinal epithelial cells [22]. Both PIP 640 and TNF-α/IFNγ treatments induced MLC-pS^{19}, but occludin down-regulation was only observed following TNF-α/IFNγ treatment (Fig. 8B).

We next compared the nature of the enhanced paracellular permeability associated with apical PIP 640 treatment to that of basolateral treatment with TNF-α/IFNγ by assessing AB transport of fluorescently-labeled dextrans with average MWs of ~ 4-, 10-, and 70-kDa, having hydrodynamic radii ~14, 23, and 60 Å, respectively (Fig. 8C). TNF-α/IFNγ enhanced the AB transport for all three dextrans in a manner inversely proportional to their molecular weight, while PIP 640 treatment resulted in AB transport enhancement that was restricted to the 4-kDa dextran (Fig. 8C). Thus, both occludin expression changes and size restrictions with regard to the size of dextrans capable of AB transport were distinct in Caco-2 monolayers *in vitro* in response to basolateral TNF-α/IFNγ compared to apical PIP 640 treatments.

PIP 640 produces a positive charge-selective bias for macromolecular transport *in vitro*

At TJs, claudin-2 can establish an ion channel that is selectively permeable to cations and water [35, 38, 39]. Since PIP 640 selectively increased claudin-2 levels at TJ structures and also effected an increase in the permeability of 4-kDa dextran, we next asked whether PIP 640mediated TJ property changes that would be biased toward the paracellular transport of positively charged macromolecules. To study this, TEER changes of Caco-2 cell monolayers and AB transport of fluorescent dextrans with either an overall positive or overall negative charge was compared to that of neutral dextran *in vitro*. Using separate monolayers, 4-kDa size forms of positively-charged diethylaminoethyl (DEAE)-dextran or negatively-charged carboxymethyl (CM)-dextran were mixed with neutral 4 kDa dextran and applied apically to Caco-2 monolayers treated with 1 mM of PIP 640 (Fig. 9). Two forms of dextran that could be distinguished based on their covalent labeling with different fluorophores were tested in each case to provide an internal control. After 60 min, the extent of AB dextran transport was determined from media collected from the basal compartment. At that time, the apical

media containing the dextrans being tested was replaced with fresh media and Caco-2 cell monolayer TEER values were monitored over the next 5 h to ensure TJ function recovery (Fig. 9A). Caco-2 monolayers treated with PIP 640 were more permeable to 4-kDa positively-charged DEAE-dextran than neutral 4kDa dextran and PIP 640-mediated paracellular permeability changes were comparable for 4kDa negatively-charged CM-dextran and 4-kDa neutral dextran (Fig. 9B). These results suggest that there is a positive-charge bias for the enhanced paracellular route induced by PIP 640 that is accessed by these dextrans.

We next asked the question of whether claudin-2 could play a role in the positive-charge bias observed for the enhanced permeability of 4-kDa dextran induced by PIP 640. To do this, we used a Caco-2 cell line with a stable knock-down (KD) for claudin-2 and compared it to a control Caco-2 cell line (CKD) in the same *in vitro* format of polarized monolayers [21]. Claudin2 KD cells, and CKD cells, retained their capacity to respond to 1 mM PIP 640 with increased levels of MLC-pS^{19} levels but in this case, there was no increase in claudin-2 levels, a response that was retained in CKD cells (Figs. 10A and B). Additionally, both KD and CKD cells responded to 1 mM PIP 640 with comparable decreases in TEER values after 60 min of apical exposure (Fig. 10C). The response in the bias toward the AB transport of positively-charged 4-kDa dextran relative to neutral or negatively-charged forms, however, was lost in the claudin-2 KD cell monolayers while being retained in the claudin-2 CKD cells (Fig. 10D). Thus, the selective AB transport of positively charged macromolecules induced by 1 mM PIP 640 is dependent upon the perm-selective properties of claudin-2.

PIP 640 modulates claudin-2 *in vivo*

In order to assess the potential change of claudin-2 in response to PIP 640 *in vivo*, studies were performed where the peptide was administered to rat jejunum by intraluminal injection (ILI). Intestinal tissues exposed to 20 mM PIP 640 for 40 min were collected and analyzed by immunoblotting and immunofluorescence microscopy to monitor the amount and cellular distribution of claudin-2. Previous studies have shown that, due to dynamic issues of dilution and motility-induced distribution of the peptide, 20 mM PIP 640 *in vivo* provided pharmacological outcomes comparable to 1 mM *in vitro* studies for PIP 640 [19, 20]. In agreement with *in vitro* data, immunoblotting analysis detected an increase in claudin-2 that was correlated with an enhancement to MLC-pS^{19} relative to total MLC levels *in vivo* (Figs. 11A and B). Expression levels and cellular distribution assessed by immunofluorescence staining demonstrated that in un-treated (control) rat intestinal tissue, claudin-2, claudin-1, and occludin all demonstrated a distribution that was greatest at the basal surface and basal segment of lateral membranes domain of the plasma membrane (Fig. 11C). Rat jejunum tissue examined 40 min after ILI of 20 mM PIP 640 showed no striking difference in the distribution of claudin-1, and occludin, but claudin-2 protein was detected to a greater extent in the apical domain of the lateral membrane of enterocytes (Fig. 11C). From this qualitative assessment of claudin-2 localization, it was not possible to determine if the increased levels of claudin-2 determined by biochemical analysis of rat jejunum in response 20 mM PIP 640 (Figs. 11A and B) reflected a greater level of claudin-2 at this apical domain of the lateral membrane or other cellular regions.

PIP 640 enhances *in vivo* uptake of therapeutic peptides with positive-charge bias

To examine the possibility that PIP 640 could produce a charge-preferential TJ permeability change *in vivo*, we planned to compare the potential for enhanced uptake of either salmon calcitonin or Exenatide; these two therapeutic peptides have similar calculated hydrodynamic radii of ~11 Å, but differ in isoelectric point (pI) values. Since salmon calcitonin has a pI of 9.3 while the pI of Exenatide is 4.9 [40, 41], their net charge at the physiological pH of the rat jejunum lumen (~5.7–7.4) would be net positive and net negative, respectively. An initial transport study with these two peptides across polarized Caco-2 monolayers *in vitro* was first performed to verify the potential for charge-selective enhancement by PIP 640 (Figs. 12A and B). Similar to *in vitro* transport studies examining positive- and negative-charged dextrans relative to neutral dextran (Fig. 9B), salmon calcitonin showed a greater enhancement of apical to basal permeability across Caco-2 monolayers induced by 1 mM PIP 640 compared to Exenatide.

These same peptides were then tested for their enhanced permeability resulting from ILI injection with or without 20 mM PIP 640 as described previously [19]. In those previous studies testing the ability of PIP 640 to enhance the paracellular permeability of insulin, 10 mM citric acid was co-administered as a way to improve the luminal stability of this peptide therapeutic [42]. Since the presence of 10 mM citric acid could significantly alter the local luminal pH at the site of ILI, potentially negating the goal of this study, 1.5 mg/mL soybean trypsin inhibitor (SBTI) was used to improve the luminal stability of salmon calcitonin or Exenatide instead of citric acid. The concentration of SBTI selected has been used to increase the stability of therapeutic peptides without inducing significant permeability enhancement [43]. Importantly, uptake of Exenatide or calcitonin (0.5 mg each) following ILI was assessed in serum obtained from portal vein blood collections, and not tail vein in order to eliminate the potential for unequal hepatic extraction.

ILI administration of PIP 640 Exenatide and salmon calcitonin in the presence of SBTI resulted in a small fraction being absorbed and reaching the portal vein, with that fraction being ~3-fold greater for Exenatide compared to salmon calcitonin (Table 1; Figs. 12C and D). Similar ILI of these two therapeutic peptides with 20 mM PIP 640 resulted in a striking enhancement of their permeability as demonstrated by portal vein time-concentrations profiles (Table 1; Figs. 12C and D). We observed that the enhanced permeability of these two therapeutic peptides induced by the co-administration of 20 mM PIP 640 were comparable, with similar maximum plasma concentration (C_{max}) at 40 min and calculated area under the curve (AUC) values (Figs. 12C and D). Portal vein concentration-time profiles suggested that salmon calcitonin concentration after 30 min of exposure were slightly higher than that obtained for Exenatide, but the difference was not statistically significant (Figs. 12C and D). For the purpose of testing the hypothesis posed for this experiment, we observed that PIP 640-mediated enhanced uptake for salmon calcitonin based upon AUC was ~10-fold relative to control, while PIP 640 enhancement of Exenatide uptake had an increase in AUC value of ~5-fold in comparison to Exenatide alone (Table 1). Although the complete pharmacokinetic (PK) parameters required to properly calculate bioavailability were not available, the AUC values presented here suggest that PIP 640 enhanced the bioavailability of positively-charged salmon calcitonin more than that of

negatively-charged Exenatide. This finding was consistent with the observed positive charge bias for transport of these therapeutic peptides across Caco-2 cell monolayers *in vitro* and the enhanced detectable amount of claudin-2 in immunoblotting data *in vivo* that induced by PIP 640.

In order to verify that these changes to MLC-pS^{19} and claudin-2 did not result in extensive paracellular permeability defects *in vivo*, the extent of PIP 640-mediated increased in serum endotoxin, i.e. lipopolysaccharide (LPS), was assessed. using a *Limulus amebocyte* lysate (LAL) assay to semi-quantitatively detect endotoxin levels in blood plasma samples collected from the portal vein (Supplementary Fig. 2). Based on this assay, endotoxin levels following PIP 640 treatment were < 0.01 EU/mL, similar to that observed for untreated (control) rats (Supplementary Figure 2).

Discussion

The intestinal epithelial barrier performs the critical task of protecting the body from invasion by harmful agents or pathogens that might induce systemic disorders and/or local inflammation to the intestine [2], while also selectively absorbing essential nutrients and foodstuff required to support the energy requirements to sustain life. The present studies have examined the nature of how that barrier can be transiently modified to provide a paracellular pathway to improve the oral bioavailability of peptide therapeutics opportunity. Previous studies have identified and characterized PIP 640, a peptide designed to inhibit MLCP as a way to increase cellular levels of MLC-pS^{19} and transiently increase the paracellular permeability of intestinal TJ structures [19, 20]. The present studies have examined the functional characteristics of the paracellular pathway generated by PIP 640 and identified the involvement of the TJ protein claudin-2 in regulating the physicochemical properties resulting from the actions of this peptide. Overall, the paracellular pathway enhanced by PIP 640 was found to have a size limit for solutes with a radius of < 23 Å, and a bias toward positively-charged macromolecular solutes that involved the TJ protein claudin-2. The data supporting these observations were obtained in both *in vitro* and *in vivo* models of trans-epithelial transport and, in sum, support a previously unreported format for altered paracellular permeability properties.

TJs are naturally permeable to ions with radii < 4 Å in a charge-selective manner with claudin family members defining the regulation of these properties [28]. These changes define the so-called pore pathway of TJ flux [36, 44]. Extensive changes to TJ protein composition can occur in response to frank damage and the ensuing repair processes, to result in an unrestricted pathway for solutes larger than 70-kDa dextran between adjacent epithelial cells [32]. In between the subtle TJ structural modifications that modulate the pore pathway and epithelial cell transitions associated with frank damage is the leak pathway associated hallmarks of TNFα/IFNγ-mediated solute permeability changes of intestinal epithelia, where solutes in the range of 4–70 kDa dextrans can transport across an epithelium [45]. In the present study, the leak pathway activated by PIP 640 resulted in a charge-selective bias similar to pore pathway events while also enhancing the permeability of solutes such as 4 kDa dextran that require engagement of the leak pathway. Thus, apical

application of PIP 640 induced TJ modifications resulting in properties that are in-between leak and pore pathway outcomes.

Although both PIP 640 and TNFα/IFNγ treatment both resulted in increased levels of MLCpS^{19}, PIP 640 selectively increased claudin-2 levels without affecting a larger number of other TJ-related protein, including occludin. Oppositely, TNFα/IFNγ treatment reduces occludin levels [46] but has no effect on claudin-2 levels or cellular localization [45]. The actions of PIP 640 reiterates the independence of claudin-2 to act at TJ structures that is distinct from other claudin proteins; for example, claudin-4 and claudin-8 or claudin-16 and claudin-19 required cis-interactions between them for effecting TJ targeting [47, 48]. Additionally, claudin-2 seems to function in homotypic trans-interactions unlike claudins-1 and −3 at TJ structures [49]. At this time, however, is it unclear if claudin-2 engages with some protein(s) not examined in these studies that could be important for its rapid apparent increase in its level observed in the immunnoblotting data and enhanced TJ localization that was inconsistent with the action of IL22 on the increased role of claudin-2 in barrier function properties [50]. Indeed, the actions of PIP 640 occurred on a time-scale of minutes while the TNFα/IFNγ actions required several hours to be observed. The rapid nature of PIP 640 actions and recovery upon withdrawal suggests a mechanism that does not require protein synthesis but rather some rapid process(es). Such events could involve suppression of claudin-2 removal from TJ structures through its reduced degradation and/or some form of post-translational modification that affects TJ targeting of this protein.

The rapid time course of claudin-2 modification induced by PIP 640 treatment was preceded by increased levels of MLC-pS^{19} relative to total cellular MLC, consistent with an endogenous mechanism suggested to provide a secondary route for nutrient uptake from the intestinal lumen through the paracellular route [14, 15, 51]. This correlation with MLC-pS^{19} provides support for the anticipated mechanism of PIP 640, as this peptide was rationally designed to mimic the inhibitory function of CPI-17 that inhibits MLCP through interactions with the MYPT1:PP1 components of the MLCP complex [19]. Importantly, a positive-charged bias for solute permeability enhanced by PIP 640 was demonstrated for different charged forms of 4-kDa dextran *in vitro* and the enhanced uptake of a positively-charged salmon calcitonin relative to a negatively-charged exenatide from the rat intestinal lumen *in vivo*. While models have been developed to explain the actions claudin-2 to provide a positive ion-selective bias for TJ structures involving the pore pathway [39], there is currently no model to account for a positive bias for macromolecular solutes through the paracellular route that requires claudin-2. Also, increased claudin-2 levels by PIP 640 was not controlled solely by increased MLC-pS^{19} levels since PIP 644, an analogue of PIP 640 increases MLC-pS^{19} levels but with reduced specificity for MLCP and greater function as a general phosphatase inhibitor, had no significant effect on claudin-2, similar to that observed with TNFα/IFNγ actions [46]. Interestingly, treatment with either raid-acting PIP 644 or slower-acting TNFα/IFNγ both resulted in enhanced paracellular transport of 70-kDa dextran. Together, these results are consistent with the idea that PIP 640, and the Na^+-nutrient cotransport-stimulated pathway of enhanced paracellular permeability it was designed to target, activates a cellular mechanism that is distinct from the actions of pro-inflammatory cytokines or general events associated with increased MLC-pS^{19} levels. These

differences may be related to TJ propinquity of increased MLCpS[19]; PIP 640, but not PIP 644, localizes at intracellular sites in close proximity to TJs [20].

PIP 640 was rationally designed to activate a pathway described in small intestinal epithelium that can result in the absorption of inert polymers such as inulin (5.5 kDa) or polyethylene glycol (4 kDa) via paracellular solvent drag that is stimulated by Na+-coupled transport of glucose or amino acids [14, 15]. Subsequent studies showed that oligopeptides in the size range of 750–900 Da could be extensively (~50%) absorbed when co-administrated with supra-physiological levels of glucose, although single amino acid charge differences in the peptides tested did not result in striking changes in paracellular transport induced by glucose [52]. Differences observed in the current studies for claudin-2-dependent enhancement of positively charged 4 kDa dextran over neutral or positively-charged forms of 4 kDa dextran *in vitro* as well as the difference between salmon calcitonin and exenatide uptake *in vivo* may have been related to a greater charge density and/or large molecular weights of these solutes that provide a more intense sieving challenge than the smaller oligopeptides examined previously.

It is interesting to consider why a positive charge-selective leak pathway would potentially be part of a mechanism of enhance macromolecular solute transport induced as part of a strategy for the intestine to optimize its capture of luminal nutrients. First, one must consider the possibility that PIP 640 does not actually activate this nutrient-driven solute uptake pathway originally identified by Pappenheimer [14, 15]. Since several lines of evidence support PIP 640 acting through this proposed pathway, claudin-2 may provide some unique selective advantages that cannot be achieved if other TJ elements were modulated during this rapid and dynamic change in paracellular permeability. One can consider the high level of lipopolysaccharides (LPS) present in the intestinal lumen that are restricted from reaching the systemic circulation via the paracellular route by TJ structures, with appreciable blood LPS levels being associated with both local and/or systemic inflammations [3]. Intact bacterial LPS has a molecular mass of 10–20 kDa and must retain their negative charge for induction of inflammatory events [53]. Importantly, we failed to observe endotoxin uptake from the rat intestine in association with the actions of PIP 640. Thus, the positive-charge selectivity resulting from increased claudin-2 in response to PIP 640 may provide some unique properties to the paracellular permeability corridor that serves a protective function to limit LPS entry into the body while this type of leak pathway mediated by PIP 640 is active.

Our studies have identified what appears to be a type of leak pathway, where transport is enhanced for moderately-sized macromolecular solutes (4-kDa dextran, but not 10-kDa dextran), but with a bias toward solutes with a net positive charge. The pathway activated by PIP 640 appears to differ from the permeation enhancing actions of 10 mM of sodium caprate where tricellulin and claudin-5 redistribution from tri-cellular and bi-cellular TJs after ~30 min correlated with enhanced permeability to molecules as large as 10-kDa dextran [9]. It should be emphasized that PIP 640 resulted in the highly selective augmentation of claudin-2; as there were no detectable changes in the other TJ protein in occludin or tricellulin or claudin-15, the last which is known to promote the passage of positively charged ions similar to claudin-2 [21, 32]. Consistent with the observation that

PIP 640 selectively enhanced positively-charged solutes over neutral or negatively-charged ones, we did not detect any alterations to claudin-4, 7 and −8, all of which have been associated with contributing to increased TJ permeability of negatively charged ions [21, 32]. We also failed to observe changes in claudins-1, −3 and −5, which have been defined to act as sealing proteins to reduce paracellular permeability [21, 32]. We assume that apical PIP 640 treatment results in activation of the leak pathway through a mechanism of increased MLC-pS^{19} levels proximate to TJ structures and established a positivecharge bias for this altered paracellular pathway through a coordinated increase of cluadin-2 at the TJ structures. These dual actions of PIP 640 to increase both MLC-pS^{19} and claudin-2 levels appear to provide its unique actions as a permeation enhancer for peptide therapeutics.

Supplementary Material

Refer to Web version on PubMed Central for supplementary material.

Acknowledgements

The authors thank the University of Hail and the Ministry of Education in Saudi Arabia for fund and support. Randy Mrsny thanks the Welcome Trust for being a Value in People recipient. Jerrold Turner was supported by US National Institutes of Health grants R01DK61931 and R01DK68271.

Abbreviations

AB	Apical-to-basolateral
AJC	Apical junctional complex
CM	Carboxymethy
DEAE	Diethylaminoethyl
DIEA	Diisopropylethylamine
FITC	Fluorescein isothiocyanate
IBD	Inflammatory bowel diseases
ILI	Intraluminal injection
IFNγ	Interferon gamma
LAL	*Limulus amebocyte* lysate
LPS	Lipopolysaccharide
MLC	Myosin light chain
MLC-pS^{19}	myosin light chain phosphorylation at serine 19
MLCP	Myosin light chain phosphatase
MoA	Mechanism of action

MYPT1	Myosin phosphatase target subunit
PBS	Phosphate buffer saline
PK	Pharmacokinetics
PP1	Protein phosphatase 1
RT	Room temperature
SBTI	Soybean trypsin inhibitor
TEER	Trans-epithelial electrical resistance
TJ	Tight junction
TNFα	Tumor necrosis factor alpha
TRITC	Tetramethylrhodamine isothiocyanate

References

[1]. Giepmans BN, van Ijzendoorn SC, Epithelial cell-cell junctions and plasma membrane domains, Biochim Biophys Acta, 1788 (2009) 820–831. [PubMed: 18706883]

[2]. Zihni C, Mills C, Matter K, Balda MS, Tight junctions: from simple barriers to multifunctional molecular gates, Nat Rev Mol Cell Biol, 17 (2016) 564–580. [PubMed: 27353478]

[3]. Vancamelbeke M, Vermeire S, The intestinal barrier: a fundamental role in health and disease, Expert Rev Gastroenterol Hepatol, 11 (2017) 821–834. [PubMed: 28650209]

[4]. Aguirre TA, Teijeiro-Osorio D, Rosa M, Coulter IS, Alonso MJ, Brayden DJ, Current status of selected oral peptide technologies in advanced preclinical development and in clinical trials, Advanced drug delivery reviews, 106 (2016) 223–241. [PubMed: 26921819]

[5]. McCartney F, Gleeson JP, Brayden DJ, Safety concerns over the use of intestinal permeation enhancers: A mini-review, Tissue Barriers, 4 (2016) e1176822. [PubMed: 27358756]

[6]. Maher S, Mrsny RJ, Brayden DJ, Intestinal permeation enhancers for oral peptide delivery, Advanced drug delivery reviews, 106 (2016) 277–319. [PubMed: 27320643]

[7]. Davies M, Pieber TR, Hartoft-Nielsen ML, Hansen OKH, Jabbour S, Rosenstock J, Effect of Oral Semaglutide Compared With Placebo and Subcutaneous Semaglutide on Glycemic Control in Patients With Type 2 Diabetes: A Randomized Clinical Trial, JAMA, 318 (2017) 1460–1470. [PubMed: 29049653]

[8]. Maher S, Leonard TW, Jacobsen J, Brayden DJ, Safety and efficacy of sodium caprate in promoting oral drug absorption: from in vitro to the clinic, Advanced drug delivery reviews, 61 (2009) 1427–1449. [PubMed: 19800376]

[9]. Krug SM, Amasheh M, Dittmann I, Christoffel I, Fromm M, Amasheh S, Sodium caprate as an enhancer of macromolecule permeation across tricellular tight junctions of intestinal cells, Biomaterials, 34 (2013) 275–282. [PubMed: 23069717]

[10]. Krug SM, Schulzke JD, Fromm M, Tight junction, selective permeability, and related diseases, Semin Cell Dev Biol, 36 (2014) 166–176. [PubMed: 25220018]

[11]. Krug SM, Hayaishi T, Iguchi D, Watari A, Takahashi A, Fromm M, Nagahama M, Takeda H, Okada Y, Sawasaki T, Doi T, Yagi K, Kondoh M, Angubindin-1, a novel paracellular absorption enhancer acting at the tricellular tight junction, J Control Release, 260 (2017) 1–11. [PubMed: 28528740]

[12]. Capaldo CT, Farkas AE, Hilgarth RS, Krug SM, Wolf MF, Benedik JK, Fromm M, Koval M, Parkos C, Nusrat A, Proinflammatory cytokine-induced tight junction remodeling through dynamic self-assembly of claudins, Mol Biol Cell, 25 (2014) 2710–2719. [PubMed: 25031428]

[13]. Turner JR, Molecular basis of epithelial barrier regulation: from basic mechanisms to clinical application, The American journal of pathology, 169 (2006) 1901–1909. [PubMed: 17148655]

[14]. Pappenheimer JR, On the coupling of membrane digestion with intestinal absorption of sugars and amino acids, The American journal of physiology, 265 (1993) G409–417. [PubMed: 8214061]

[15]. Madara JL, Pappenheimer JR, Structural basis for physiological regulation of paracellular pathways in intestinal epithelia, The Journal of membrane biology, 100 (1987) 149–164. [PubMed: 3430571]

[16]. Pappenheimer JR, Reiss KZ, Contribution of solvent drag through intercellular junctions to absorption of nutrients by the small intestine of the rat, The Journal of membrane biology, 100 (1987) 123–136. [PubMed: 3430569]

[17]. Turner JR, Madara JL, Physiological regulation of intestinal epithelial tight junctions as a consequence of Na(+)-coupled nutrient transport, Gastroenterology, 109 (1995) 1391–1396. [PubMed: 7557112]

[18]. Turner JR, Rill BK, Carlson SL, Carnes D, Kerner R, Mrsny RJ, Madara JL, Physiological regulation of epithelial tight junctions is associated with myosin light-chain phosphorylation, The American journal of physiology, 273 (1997) C1378–1385. [PubMed: 9357784]

[19]. Taverner A, Dondi R, Almansour K, Laurent F, Owens SE, Eggleston IM, Fotaki N, Mrsny RJ, Enhanced paracellular transport of insulin can be achieved via transient induction of myosin light chain phosphorylation, J Control Release, 210 (2015) 189–197. [PubMed: 25980620]

[20]. Almansour K, Taverner A, Eggleston IM, Mrsny RJ, Mechanistic studies of a cellpermeant peptide designed to enhance myosin light chain phosphorylation in polarized intestinal epithelia, J Control Release, (2018).

[21]. Weber CR, Liang GH, Wang Y, Das S, Shen L, Yu AS, Nelson DJ, Turner JR, Claudin-2dependent paracellular channels are dynamically gated, Elife, 4 (2015) e09906. [PubMed: 26568313]

[22]. Wang F, Schwarz BT, Graham WV, Wang Y, Su L, Clayburgh DR, Abraham C, Turner JR, IFN-gamma-induced TNFR2 expression is required for TNF-dependent intestinal epithelial barrier dysfunction, Gastroenterology, 131 (2006) 1153–1163. [PubMed: 17030185]

[23]. Venturoli D, Rippe B, Ficoll and dextran vs. globular proteins as probes for testing glomerular permselectivity: effects of molecular size, shape, charge, and deformability, Am J Physiol Renal Physiol, 288 (2005) F605–613. [PubMed: 15753324]

[24]. Zhang Y, Huo M, Zhou J, Xie S, PKSolver: An add-in program for pharmacokinetic and pharmacodynamic data analysis in Microsoft Excel, Comput Methods Programs Biomed, 99 (2010) 306–314. [PubMed: 20176408]

[25]. Clayburgh DR, Barrett TA, Tang Y, Meddings JB, Van Eldik LJ, Watterson DM, Clarke LL, Mrsny RJ, Turner JR, Epithelial myosin light chain kinase-dependent barrier dysfunction mediates T cell activation-induced diarrhea in vivo, The Journal of clinical investigation, 115 (2005) 2702–2715. [PubMed: 16184195]

[26]. Raleigh DR, Marchiando AM, Zhang Y, Shen L, Sasaki H, Wang Y, Long M, Turner JR, Tight junction-associated MARVEL proteins marveld3, tricellulin, and occludin have distinct but overlapping functions, Mol Biol Cell, 21 (2010) 1200–1213. [PubMed: 20164257]

[27]. Umeda K, Matsui T, Nakayama M, Furuse K, Sasaki H, Furuse M, Tsukita S, Establishment and characterization of cultured epithelial cells lacking expression of ZO-1, The Journal of biological chemistry, 279 (2004) 44785–44794. [PubMed: 15292177]

[28]. Lingaraju A, Long TM, Wang Y, Austin, JR, 2nd, Turner JR, Conceptual barriers to understanding physical barriers, Semin Cell Dev Biol, 42 (2015) 13–21. [PubMed: 26003050]

[29]. Furuse M, Hata M, Furuse K, Yoshida Y, Haratake A, Sugitani Y, Noda T, Kubo A, Tsukita S, Claudin-based tight junctions are crucial for the mammalian epidermal barrier: a lesson from claudin-1-deficient mice, J Cell Biol, 156 (2002) 1099–1111. [PubMed: 11889141]

[30]. Zeissig S, Burgel N, Gunzel D, Richter J, Mankertz J, Wahnschaffe U, Kroesen AJ, Zeitz M, Fromm M, Schulzke JD, Changes in expression and distribution of claudin 2, 5 and 8 lead to discontinuous tight junctions and barrier dysfunction in active Crohn's disease, Gut, 56 (2007) 61–72. [PubMed: 16822808]

[31]. Barmeyer C, Schulzke JD, Fromm M, Claudin-related intestinal diseases, Semin Cell Dev Biol, 42 (2015) 30–38. [PubMed: 25999319]

[32]. Lu Z, Ding L, Lu Q, Chen YH, Claudins in intestines: Distribution and functional significance in health and diseases, Tissue Barriers, 1 (2013) e24978. [PubMed: 24478939]

[33]. Lu R, Johnson DL, Stewart L, Waite K, Elliott D, Wilson JM, Rab14 regulation of claudin2 trafficking modulates epithelial permeability and lumen morphogenesis, Mol Biol Cell, 25 (2014) 1744–1754. [PubMed: 24694596]

[34]. Van Itallie CM, Tietgens AJ, LoGrande K, Aponte A, Gucek M, Anderson JM, Phosphorylation of claudin-2 on serine 208 promotes membrane retention and reduces trafficking to lysosomes, J Cell Sci, 125 (2012) 4902–4912. [PubMed: 22825868]

[35]. Amasheh S, Meiri N, Gitter AH, Schoneberg T, Mankertz J, Schulzke JD, Fromm M, Claudin-2 expression induces cation-selective channels in tight junctions of epithelial cells, J Cell Sci, 115 (2002) 4969–4976. [PubMed: 12432083]

[36]. Turner JR, Intestinal mucosal barrier function in health and disease, Nat Rev Immunol, 9 (2009) 799–809. [PubMed: 19855405]

[37]. Zolotarevsky Y, Hecht G, Koutsouris A, Gonzalez DE, Quan C, Tom J, Mrsny RJ, Turner JR, A membrane-permeant peptide that inhibits MLC kinase restores barrier function in in vitro models of intestinal disease, Gastroenterology, 123 (2002) 163–172. [PubMed: 12105845]

[38]. Rosenthal R, Milatz S, Krug SM, Oelrich B, Schulzke JD, Amasheh S, Gunzel D, Fromm M, Claudin-2, a component of the tight junction, forms a paracellular water channel, J Cell Sci, 123 (2010) 1913–1921. [PubMed: 20460438]

[39]. Yu AS, Cheng MH, Angelow S, Gunzel D, Kanzawa SA, Schneeberger EE, Fromm M, Coalson RD, Molecular basis for cation selectivity in claudin-2-based paracellular pores: identification of an electrostatic interaction site, J Gen Physiol, 133 (2009) 111–127. [PubMed: 19114638]

[40]. Chan HK, Clark AR, Feeley JC, Kuo MC, Lehrman SR, Pikal-Cleland K, Miller DP, Vehring R, Lechuga-Ballesteros D, Physical stability of salmon calcitonin spray-dried powders for inhalation, Journal of pharmaceutical sciences, 93 (2004) 792–804. [PubMed: 14762916]

[41]. Kim JY, Lee H, Oh KS, Kweon S, Jeon OC, Byun Y, Kim K, Kwon IC, Kim SY, Yuk SH, Multilayer nanoparticles for sustained delivery of exenatide to treat type 2 diabetes mellitus, Biomaterials, 34 (2013) 8444–8449. [PubMed: 23895999]

[42]. Welling SH, Hubalek F, Jacobsen J, Brayden DJ, Rahbek UL, Buckley ST, The role of citric acid in oral peptide and protein formulations: relationship between calcium chelation and proteolysis inhibition, European journal of pharmaceutics and biopharmaceutics : official journal of Arbeitsgemeinschaft fur Pharmazeutische Verfahrenstechnik e.V, 86 (2014) 544–551.

[43]. Yamamoto A, Taniguchi T, Rikyuu K, Tsuji T, Fujita T, Murakami M, Muranishi S, Effects of various protease inhibitors on the intestinal absorption and degradation of insulin in rats, Pharmaceutical research, 11 (1994) 1496–1500. [PubMed: 7855059]

[44]. Anderson JM, Van Itallie CM, Physiology and function of the tight junction, Cold Spring Harb Perspect Biol, 1 (2009) a002584. [PubMed: 20066090]

[45]. Turner JR, Buschmann MM, Romero-Calvo I, Sailer A, Shen L, The role of molecular remodeling in differential regulation of tight junction permeability, Semin Cell Dev Biol, 36 (2014) 204–212. [PubMed: 25263012]

[46]. Bruewer M, Luegering A, Kucharzik T, Parkos CA, Madara JL, Hopkins AM, Nusrat A, Proinflammatory cytokines disrupt epithelial barrier function by apoptosis-independent mechanisms, Journal of immunology, 171 (2003) 6164–6172.

[47]. Hou J, Renigunta A, Gomes AS, Hou M, Paul DL, Waldegger S, Goodenough DA, Claudin-16 and claudin-19 interaction is required for their assembly into tight junctions and for renal reabsorption of magnesium, Proceedings of the National Academy of Sciences of the United States of America, 106 (2009) 15350–15355. [PubMed: 19706394]

[48]. Hou J, Renigunta A, Yang J, Waldegger S, Claudin-4 forms paracellular chloride channel in the kidney and requires claudin-8 for tight junction localization, Proceedings of the National Academy of Sciences of the United States of America, 107 (2010) 18010–18015. [PubMed: 20921420]

[49]. Furuse M, Sasaki H, Tsukita S, Manner of interaction of heterogeneous claudin species within and between tight junction strands, J Cell Biol, 147 (1999) 891–903. [PubMed: 10562289]

[50]. Tsai PY, Zhang B, He WQ, Zha JM, Odenwald MA, Singh G, Tamura A, Shen L, Sailer A, Yeruva S, Kuo WT, Fu YX, Tsukita S, Turner JR, IL-22 Upregulates Epithelial Claudin-2 to Drive Diarrhea and Enteric Pathogen Clearance, Cell Host Microbe, 21 (2017) 671–681 e674. [PubMed: 28618266]

[51]. Pappenheimer JR, Dahl CE, Karnovsky ML, Maggio JE, Intestinal absorption and excretion of octapeptides composed of D amino acids, Proceedings of the National Academy of Sciences of the United States of America, 91 (1994) 1942–1945. [PubMed: 8127911]

[52]. Pappenheimer JR, Karnovsky ML, Maggio JE, Absorption and excretion of undegradable peptides: role of lipid solubility and net charge, The Journal of pharmacology and experimental therapeutics, 280 (1997) 292–300. [PubMed: 8996209]

[53]. Schromm AB, Brandenburg K, Loppnow H, Zahringer U, Rietschel ET, Carroll SF, Koch MH, Kusumoto S, Seydel U, The charge of endotoxin molecules influences their conformation and IL-6-inducing capacity, Journal of immunology, 161 (1998) 5464–5471.

Highlights

- PIP 640 peptide induced a type of leak pathway that enhaces intestinal epithelial TJ permeability for moderately-sized solutes *in vitro* and *in vivo*.
- The epithelial TJ permeability induced by PIP 640 peptide is activated by a mechanism involves enhancing MLC-pS^{19} levels that results in an increase of claudin-2 at TJ structures.
- Claudin-2 increase at TJ structures associated with PIP 640 actions establishes a preferential TJ permeability to positively-charged solutes over neutral or negativelycharged ones *in vitro* and *in vivo*.

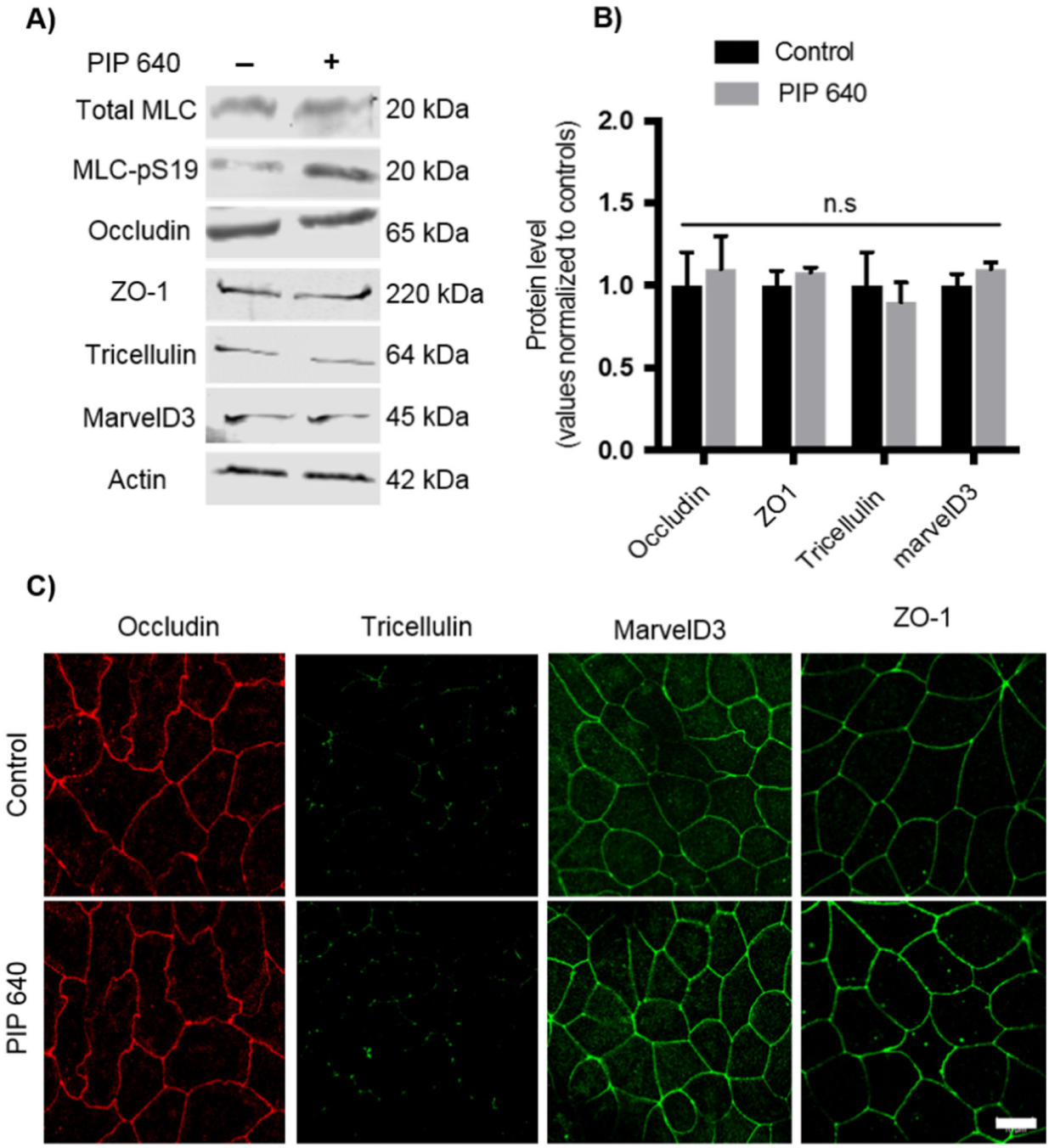

Figure 1.

PIP 640 fails to affect cellular levels or distribution of TAMPs (occludin, tricellulin, and marvelD3) as well as the scaffolding protein ZO-1 in Caco-2 cell monolayers in vitro. A) Representative immunoblots of TAMPS and ZO-1 total protein levels showed no striking changes following a 60-min apical exposure of 1 mM PIP 640; conditions that increased MLC-pS^{19} relative to total MLC levels. B) Quantitative analysis of immunoblots as shown in A); data are means ± SEM of 3 independent experiments, n=6 for control and treated monolayers. C) Immunofluorescence microscopy images demonstrated no dramatic

differences in localization of TAMPs and ZO-1 had not changed following a 60min apical exposure of 1 mM PIP 640 compared to untreated Caco-2 monolayers in vitro. Images are representative of 3 independent experiments, n=3. Scale bar, 10 μm.

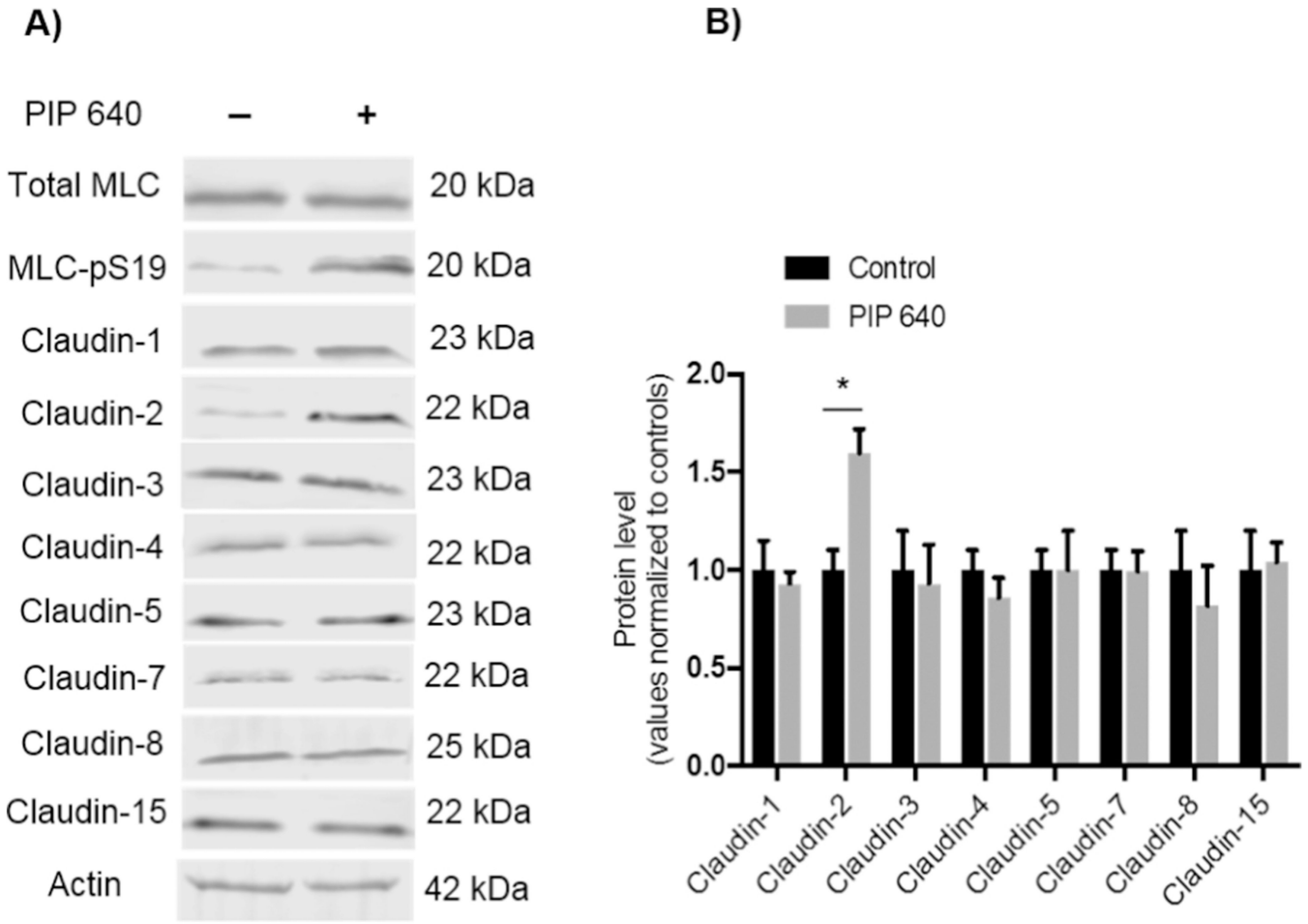

Figure 2.

Apical treatment of Caco-2 monolayers with 1 mM of PIP 640 for 60 min selectively increases cellular levels of claudin-2 protein. **A)** Immunoblotting analysis showing the effect of MLC-pS^{19} relative to total MLC induced by PIP 640 on cellular levels of claudin-1, −2, −3, −4, −5, −7, −8 and −15 that are commonly expressed by cells of the human intestinal epithelium. **B)** Quantitative analysis of the immunoblots obtained in A). Data are means ± SEM of 3 independent experiments, n=6 for the control and treated monolayers, (**p* value< 0.05).

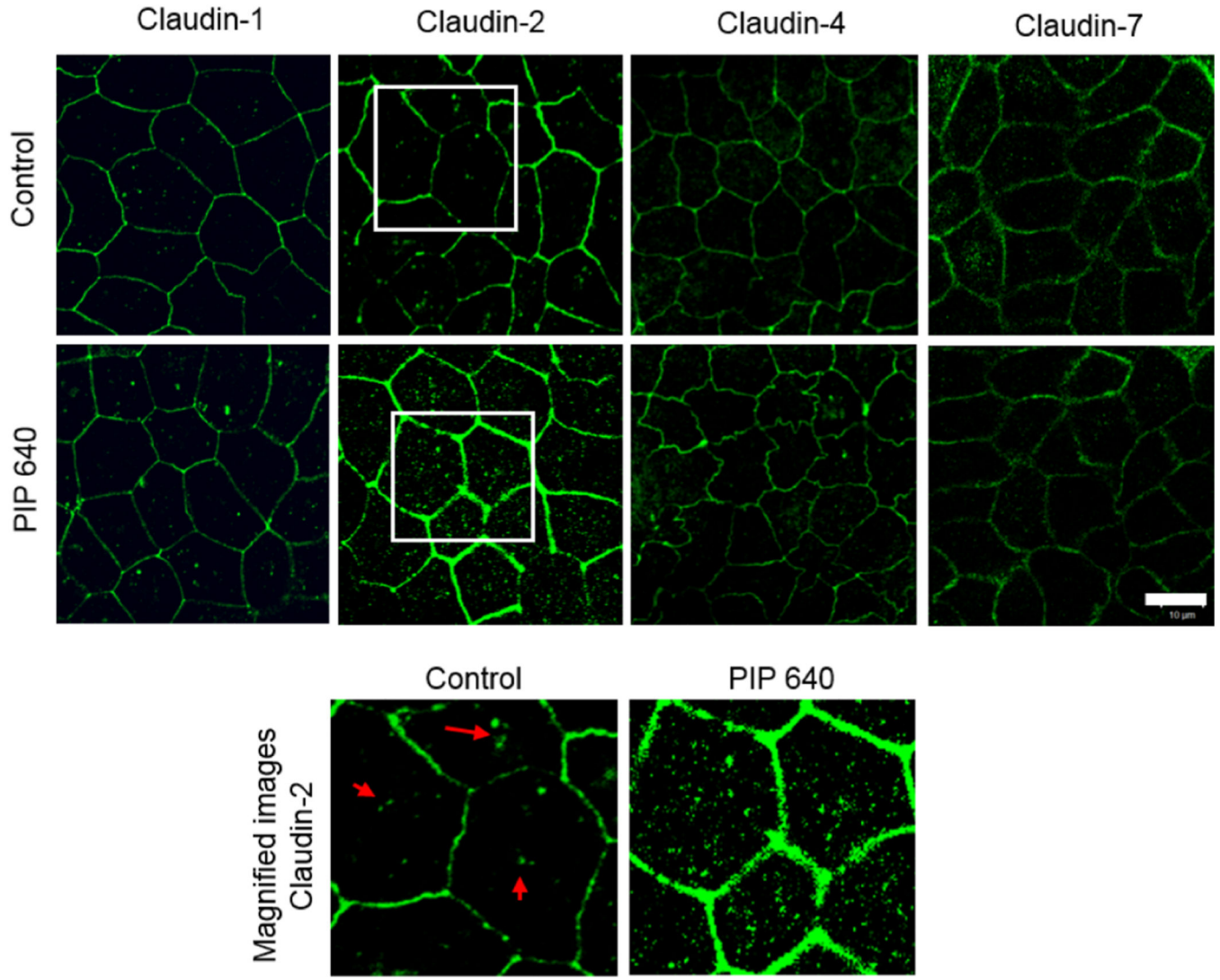

Figure 3.

Immunofluorescent images of Caco-2 monolayers showing cellular localization of claudin-1, −2, −4 and −7 before (top row) and after (middle row) exposure to the PIP 640. Areas highlighted as white boxes in the top and middle rows are shown in the bottom row at increase magnification with intracellular locations of claudin-2 in untreated Caco-2 cell monolayers highlighted by red arrows. Images are representative of 3 independent experiments, n=3. Scale bar, 10 μm.

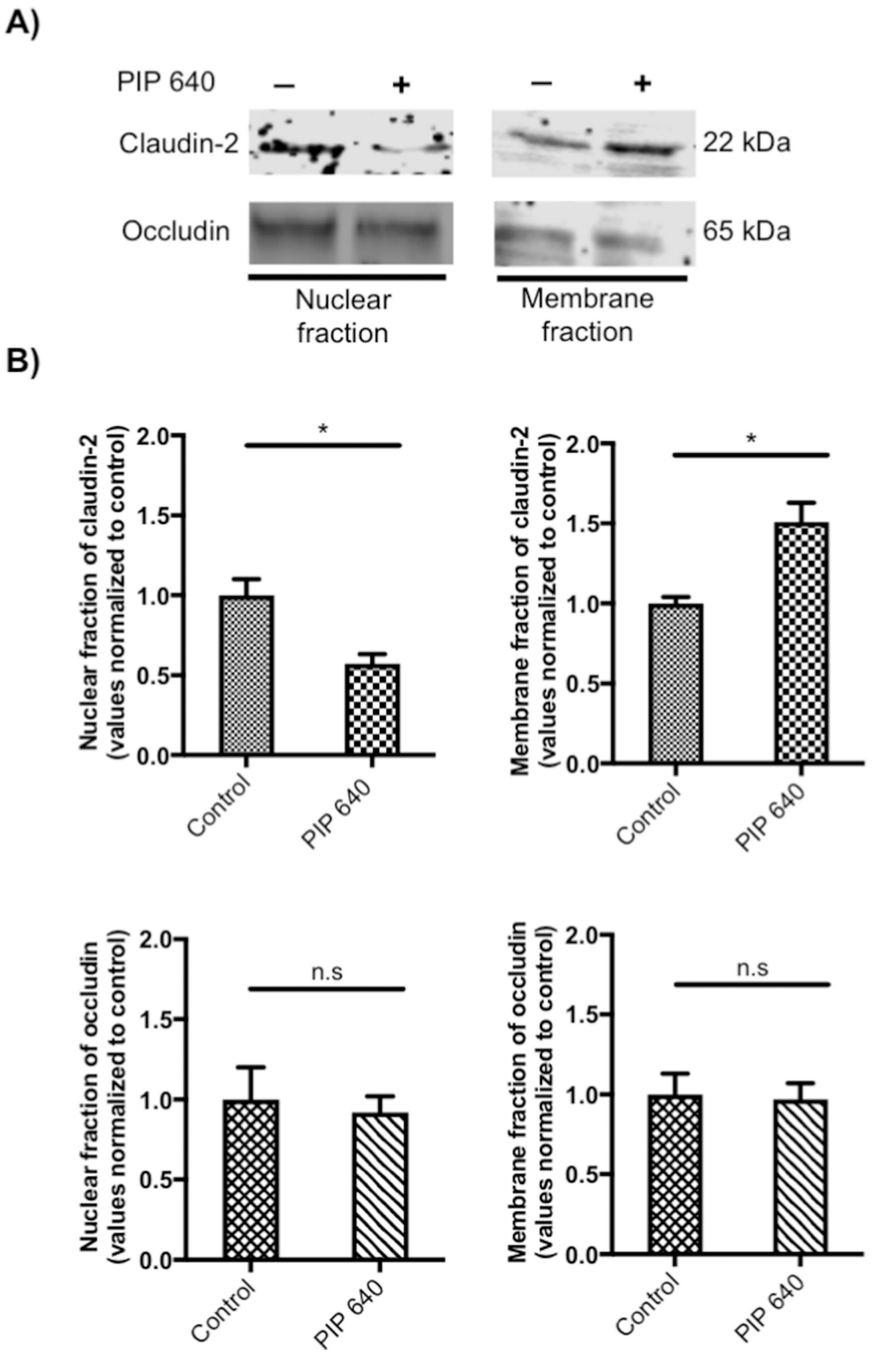

Figure 4.

PIP 640-mediated shift in distribution of claudin-2 from nuclear to membrane fractions. Confluent Caco-2 cell monolayers were gently disrupted 60 min after an apical application of 1 mM PIP 640 *in vitro*. **A)** Representative immunoblots for claudin-2 and occludin content in isolated nuclear and membrane fractions. **B)** Quantification of immunoblot band intensity for the relative levels of claudin-2 and occludin following this PIP 640 treatment. Data are means ± SEM of 3 independent experiments, n=3 for the control and treated monolayers, (**p* value< 0.05).

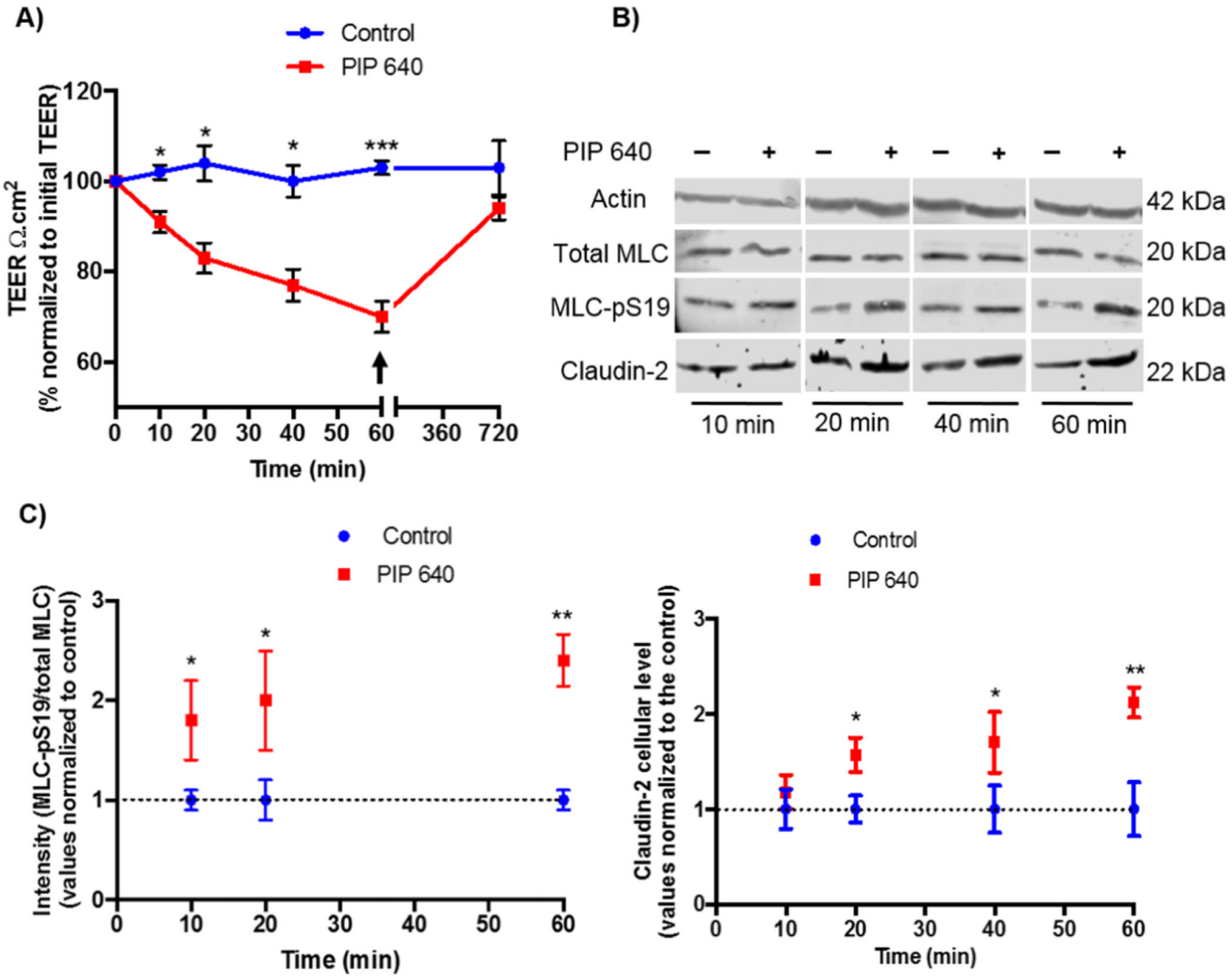

Figure 5.

Time-course assessment claudin-2 and MLC-pS^{19} levels with relation to changes in transepithelial electrical resistance (TEER) resistance in Caco-2 cell monolayers following apical treatment with 1 mM PIP 640 *in vitro*. A) TEER changes induced by 1 mM of PIP 640 over 60-min exposure following by recovery initiated by the removal of apical PIP 640 (arrow) and replacement with fresh media. **B)** Representative immunoblots showing MLC-pS^{19} levels relative to total MLC and claudin-2 levels over time following apical application of 1 mM PIP 640. **C)** Quantitative analysis of immunoblots obtained for MLC-pS^{19} and claudin-2 induced by 1 mM PIP 640. Data points represent means ± SEM of 3 independent experiments with n=6 for TEER data, n= 3 for both MLC-pS^{19} and claudin-2 immunoblotting data at all time points, immunoblot data obtained for MLC-pS^{19} for 40 min exposure n=1 (**p* value< 0.05, ***p* value< 0.01 and ****p* value<0.001).

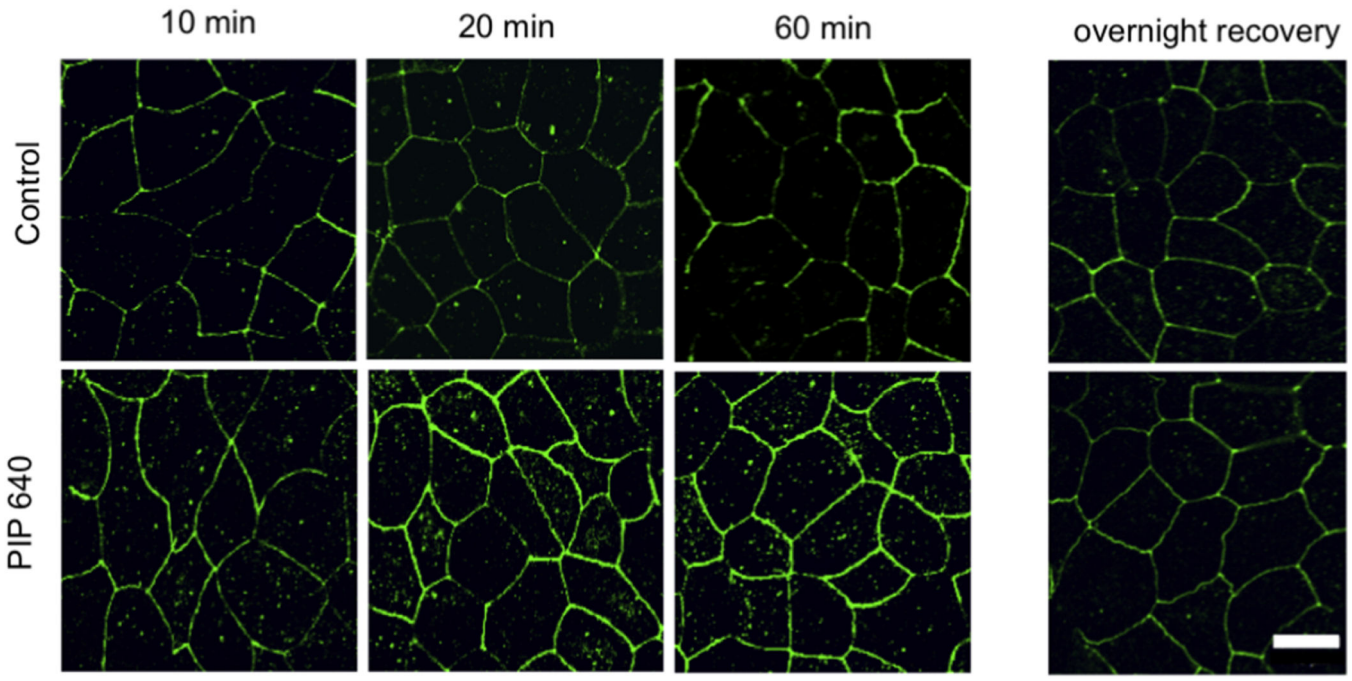

Figure 6.

Changes in the cellular claudin-2 distribution in Caco-2 monolayers over time as assessed by immunofluorescence microscopy following apical exposure to 1 mM PIP 640. Images are representative of 3 independent experiments, n=3. Scale bar, 10 μm.

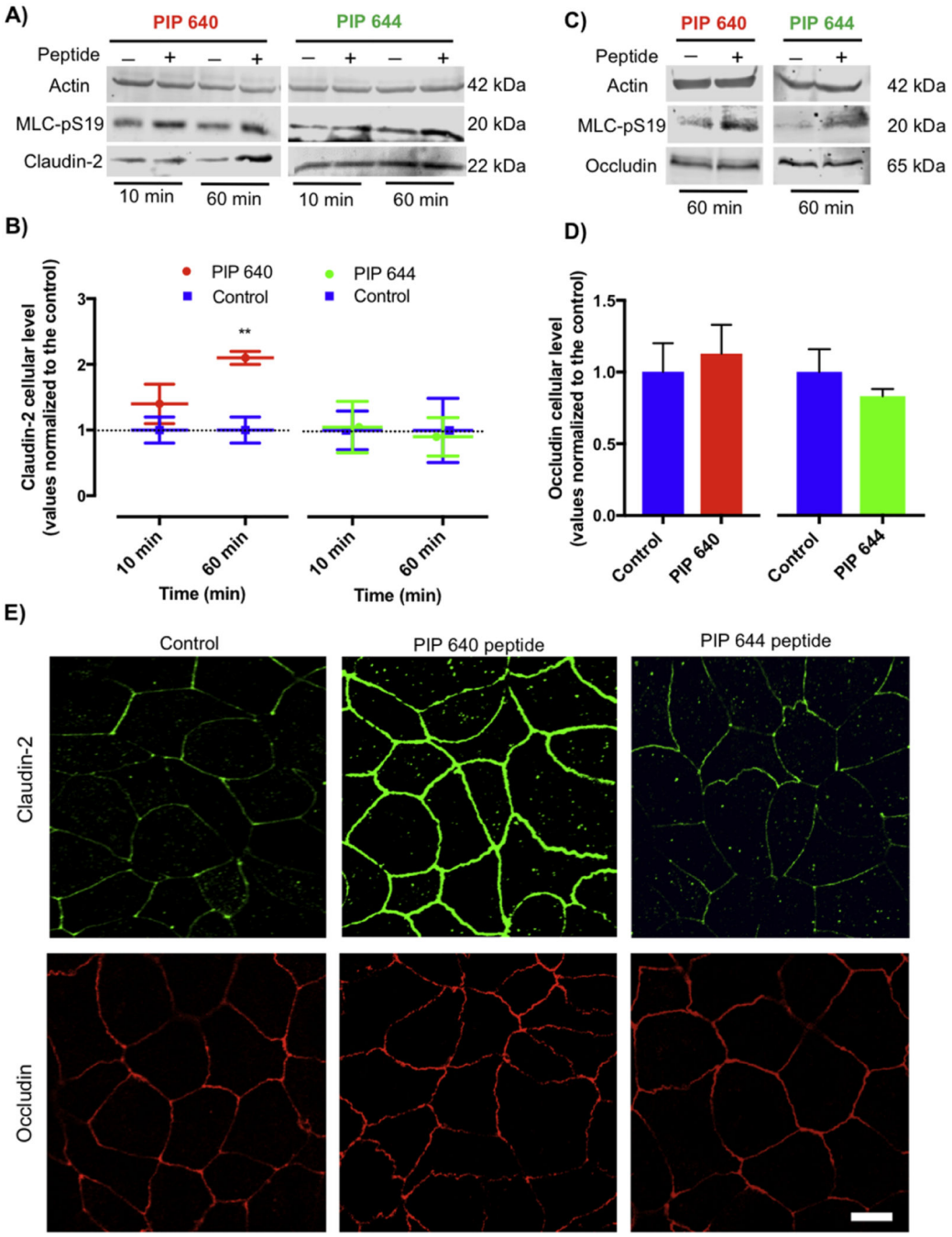

Figure 7.

Actions of PIP 644 are distinct from PIP 640 on Caco-2 cell monolayers *in vitro*. **A)** Representative immunoblots showing cellular levels of MLC-pS^{19} and claudin-2 at 10 and 60 min following apical application of 1 mM of PIP 640 or PIP 644. **B)** Quantitative analysis of immunoblots obtained for MLC-pS^{19} and claudin-2 induced by PIP 640 or PIP 644 represented in A). **C)** Representative immunoblots showing cellular levels of MLC-pS^{19} and occludin at 60 min following apical application of 1 mM of PIP 640 or PIP 644. **D)** Quantitative analysis of immunoblots obtained for MLC-pS^{19} and occludin induced by PIP

640 or PIP 644 represented in C). Data represent means ± SEM of 3 independent experiments with n=3 for both MLC-pS^{19} and claudin-2 immunoblotting data at all time points (***p* value< 0.01). **E)** Immunofluorescent staining of claudin-2 and occludin in Caco-2 cell monolayers treated with PIP 640 or PIP 644 for 60 min. Images are representative of 3 independent experiments, n=3. Scale bar, 10 μm

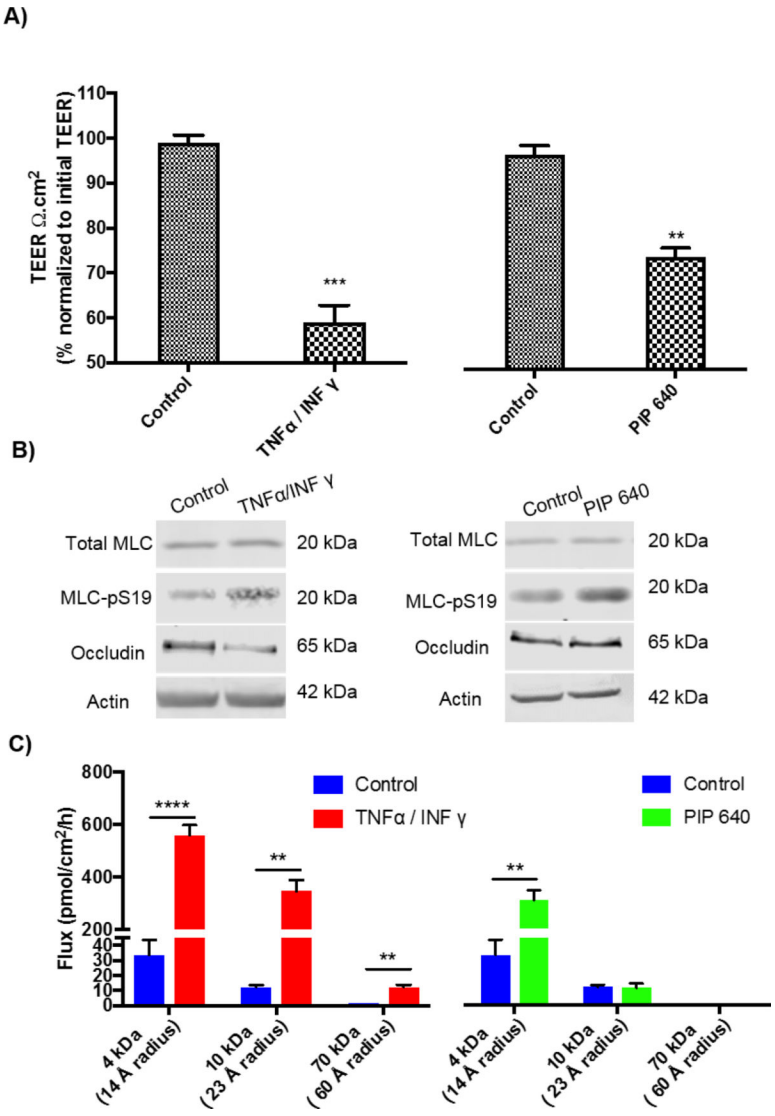

Figure 8.

Actions of PIP 640 on Caco-2 cell monolayers are distinct from those of the pro-inflammatory cytokines TNF-α/INFγ. or trans-epithelial electrical resistance (TEER) and occludin protein levels. **A)** Caco-2 monolayer TEER value changes after 60 min of apical exposure to 1 mM of PIP 640 or after 4h of basal exposure to TNF-α (5 ng/mL)/ INF-γ (10 ng/mL). Data represent means ± SEM of 3 independent experiments, with n=9 (***p* value< 0.01 and ****p* value< 0.001). **B)** Representative immunoblots demonstrating MLC-pS^{19} and occludin level changes induced by PIP 640 or TNF-α/INF-γ treatments described in **A)**. Data are representative of 4 independent experiments, n=4. (***p* value< 0.01 and * ****p* value<0.0001). **C)** Paracellular permeability changes of polarized Caco-2 monolayers *in vitro* after 4 h of basal treatment with TNF-α (5 ng/mL)/ INF-γ (10 ng/mL) or 1 h of apical treatment of 1 mM PIP 640. The extent of fluorescent dextran (4-kDa, 10-kDa and 70-kDa) apical to basal transport was determined after 60 min. Data are means ± SEM of 3 independent experiments, with n=9 (***p* value< 0.01 and *****p* value<0.0001).

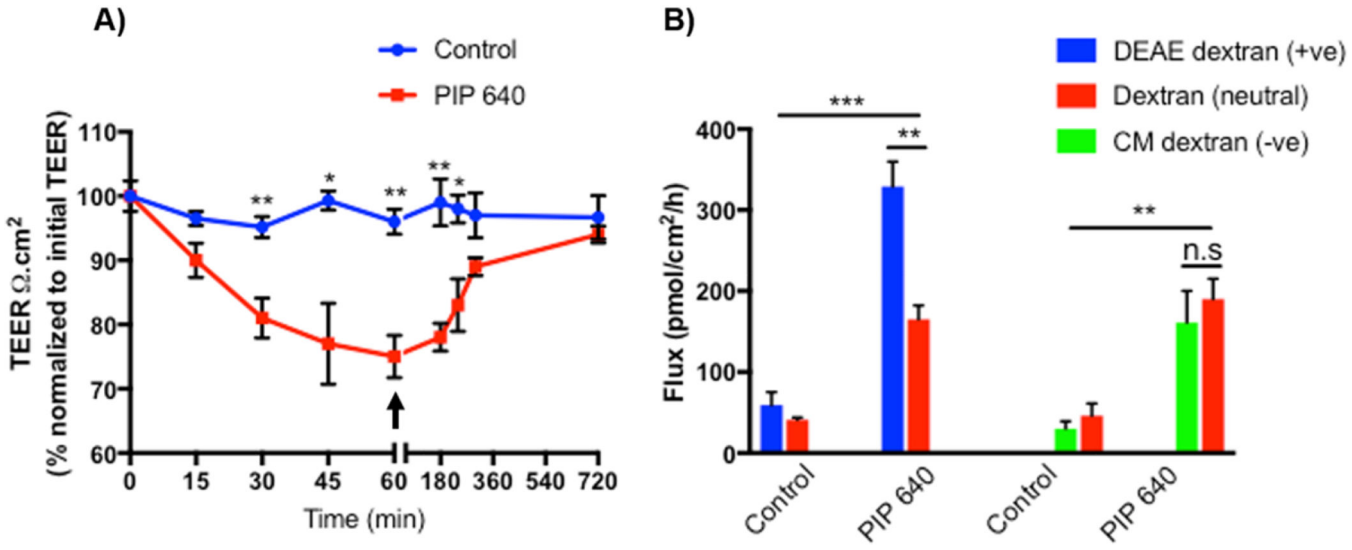

Figure 9.

PIP 640 selectively enhances apical to basal paracellular permeability of positively-charged dextran *in vitro*. **A)** Demonstration of reversibility of TEER values following washout 60 min after apical exposure to 1 mM PIP 640 in Caco-2 cells monolayer used to assess dextran permeability. **B)** Cumulative apical to basal transport after 60 min of positively-charged DEAE-dextran (+ve) or negatively-charged CM-dextran (-ve) compared to neutral dextran (all 4-kDa in size). Data are means ± SEM (**P* < 0.05, ***P* < 0.01 and ****P* <0.001).

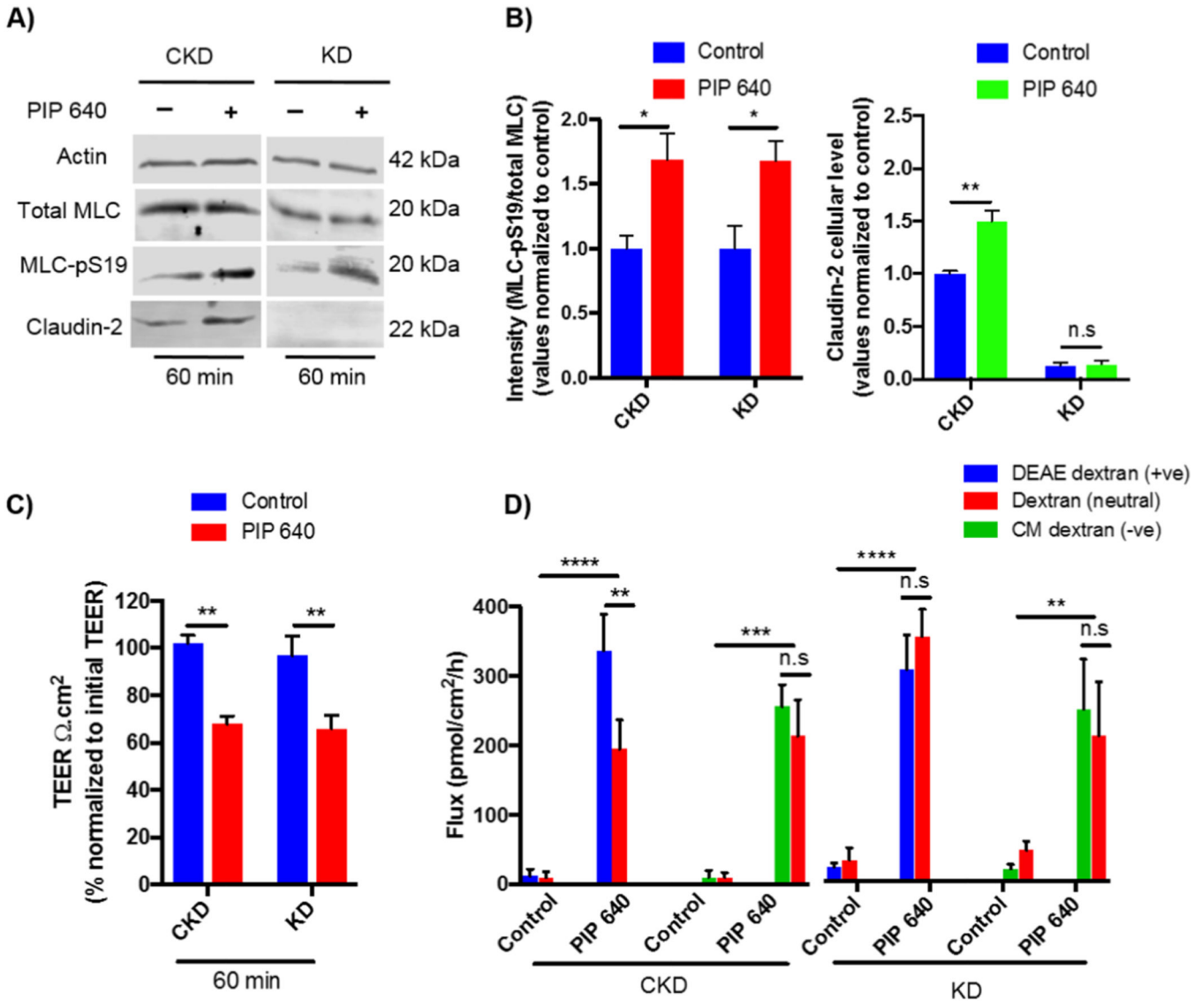

Figure 10.

The positive charge bias of paracellular permeability enhanced by PIP 640 is dependent upon claudin-2 expression. **A)** Representative immunoblots demonstrating changes in MLC-pS[19] and claudin-2 levels 60 min after apical application of 1 mM of PIP 640 to claudin-2 knock-down Caco-2 (KD) or control Caco-2 knock-down (CKD) cell monolayers *in vitro*. **B)** Quantitative analysis of changes in MLC-pS[19] and claudin-2 induced by PIP 640 shown in **A)**. **C)** Changes in TEER relative to initial values 60 min after apical application of 1 mM PIP 640 to CKD or KD Caco-2 cell monolayers. **D)** Cumulative apical to basal transport across Caco-2 monolayers of fluorescent DEAE-dextran (+ve) or CM-dextran (-ve) compared to neutral dextran (all 4-kDa in size) 60 min after apical application of 1 mM PIP 640. Data are means ± SEM of 3 independent experiments, with n=6 (*$P < 0.05$ and **$P < 0.01$, ***$P < 0.001$, ****$P < 0.0001$).

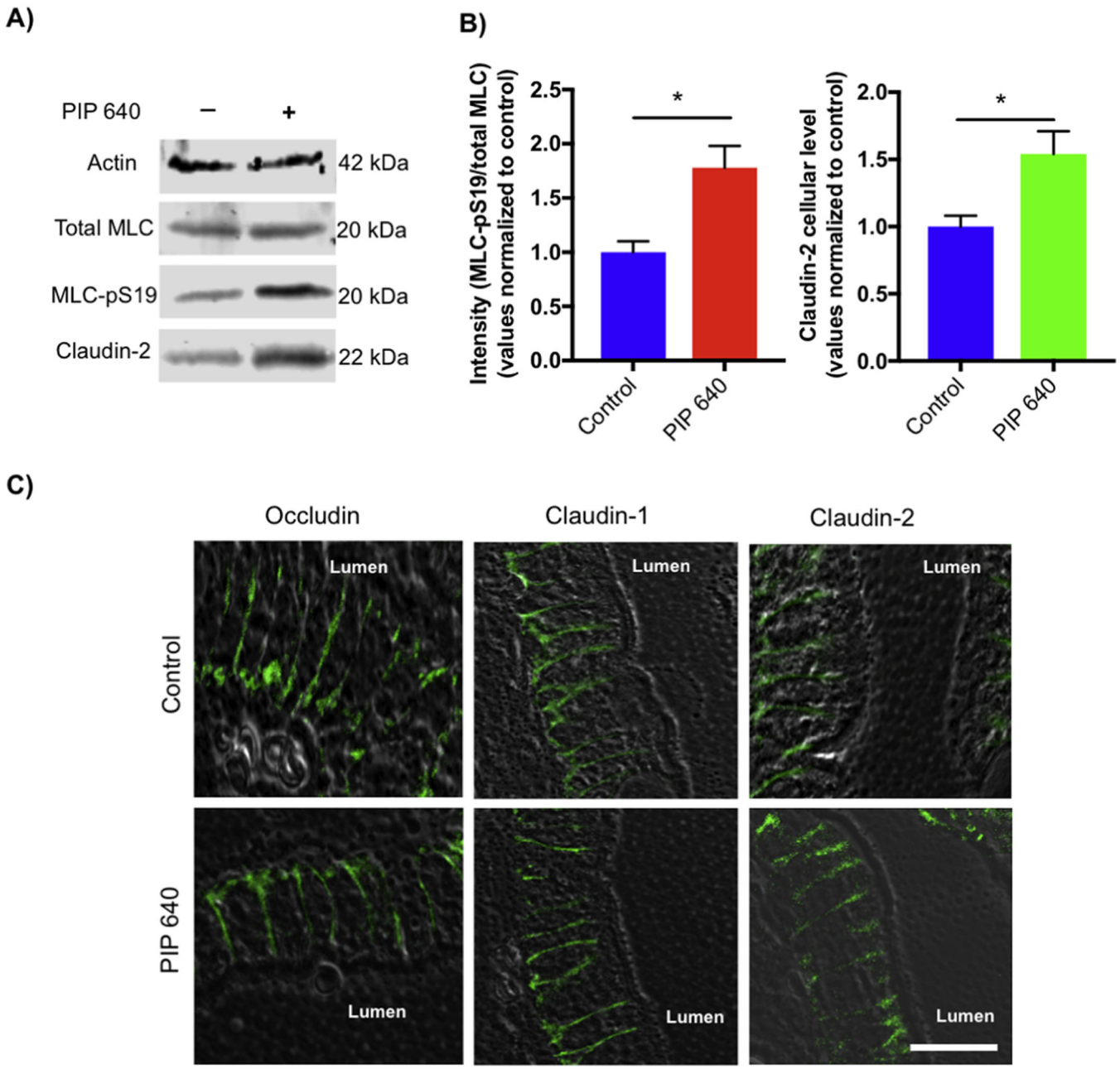

Figure 11.

PIP 640 modulates claudin-2 expression and enterocyte distribution in rat jejunum *in vivo.* **A)** Representative immunoblots showing total MLC, MLC-pS^{19} and claudin-2 levels 40 min after intra-luminal injection of 20 mM PIP 640. **B)** Quantitative analysis of immunoblots demonstrated statistically significant increases in MLC-pS^{19} relative to total MLC and claudin-2 described in **A)**. Data are means ± SEM of 3 independent experiments; n= 3. (*p value< 0.05). **C)** Claudin-2 observed in rat jejunum enterocytes using immunofluorescence microscopy shifted from a basal to more apical domain of the lateral plasma membrane in response to PIP 640, while the lateral plasma membrane distribution of claudin-1 and

occludin did not undergo this shift in response to the peptide. Images are representative of 3 independent experiments, n=3. Scale bar, 20 μm.

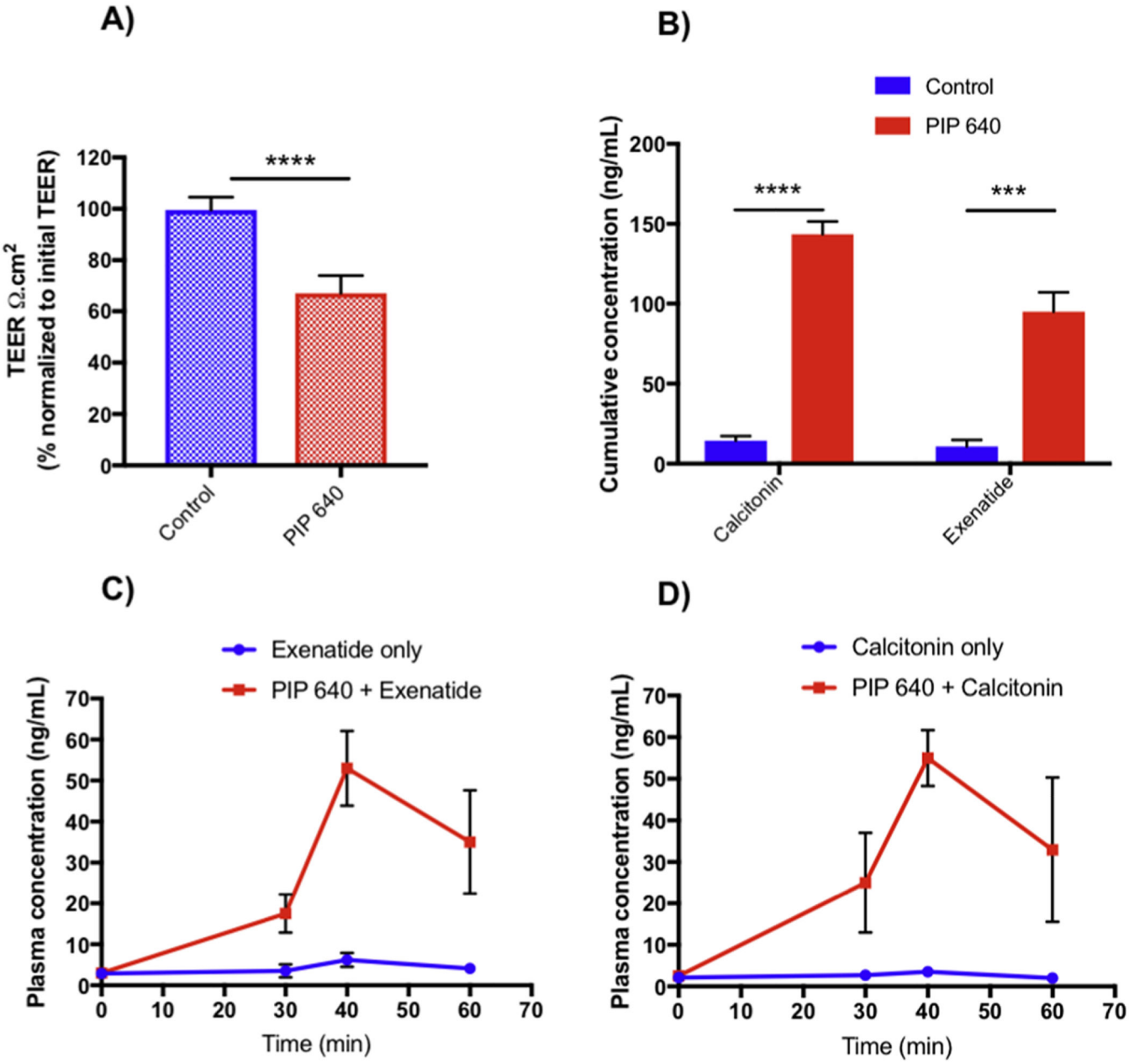

Figure 12.

PIP 640 enhances the transport of a positively-charged therapeutic peptides *in vitro* and *in vivo*. **A)** Changes in TEER relative to initial values 60 min after apical application of 1 mM PIP 640 to Caco2 cell monolayers. **B)** Cumulative apical to basal transport across polarized Caco-2 cell monolayers *in vitro* of exenatide and salmon calcitonin after 60 min. Data are means ± SEM of 3 independent experiments, with n=6 (***$P < 0.001$, ****$P < 0.0001$). Portal vein concentration-time profiles of **C)** Exenatide and **D)** salmon calcitonin following *in vivo* ILI with or without 20 mM PIP 640. Data are means ± SEM of 3 independent experiments; n= 3. One-way ANOVA indicated a significant difference between the data sets (***p* value< 0.01).

Table 1.

Physicochemical properties and portal vein PK parameters following intraluminal injection of salmon calcitonin or Exenatide with PIP 640 or without (control) into rat jejunum.

Peptide drug	MW (kDa)	Hydrodynamic size (Å)(calculated)	$AUC_{(t\ 0–60)}$ (ng/ml*min)		C_{max} (ng/ml)	
			Control	PIP 640	Control	PIP 640
Calcitonin	3.4	11	155±2.7	1680±540	3.3±0.36	55.6±6.7
Exenatide	4.2	11	237.6±38	1577±72.3	6.5±0.75	53±5.8

MW = molecular weight. The hydrodynamic radius was calculated using the relationship established between the MW and the hydrodynamic radius of a protein. PK parameters for area under the curve between 0–60 min ($AUC_{t\ 0–60}$) and maximum concentration achieved (Cmax) were calculated with the trapezoid rule using Microsoft Excel add-in program, PK-Solver [24].